



FFW

IN THE UNITED STATES PATENT AND TRADEMARK OFFICE

Applicant: Peter D. BREWER	) Examiner: Thanhha S. Pham
	)
Serial No.: 10/787,276	) Art Unit: 2813
	)
Filed: February 25, 2004	) Our Ref: B-4712 620052-7
	)
For: "SELF-MASKING DEFECT REMOVING METHOD"	) Date: May 11, 2007

**RE-SUBMISSION OF SUPPLEMENTAL DECLARATION OF PETER D. BREWER**


Mail Stop Amendment  
Commissioner for Patents  
P.O. Box 1450  
Alexandria, VA 22313-1450

Sir:


This paper accompanies the Supplemental Declaration, with the original of the signature of the applicant, Dr. Peter Brewer. The declaration includes the Exhibits A, B, and C that were inadvertently omitted when this declaration was first mailed to the Office on May 4, 2007 as part of the response to the office action of January 10, 2007.

I hereby certify that this correspondence is being deposited with the United States Post Service with sufficient postage as first class mail in an envelope addressed to: Mail Stop Amendment, Commissioner for Patents, P.O. Box 1450, Alexandria, VA 22313-1450 on May 11, 2007.

Respectfully submitted,

  
 \_\_\_\_\_  
 Lucy C. Derby  
 (name of person signing)

May 11, 2007  
 \_\_\_\_\_  
 (Date)

  
 \_\_\_\_\_  
 R. Dabney Eastham  
 Attorney for Applicants  
 Reg. No. 31,247  
 LADAS & PARRY LLP  
 5670 Wilshire Boulevard, Suite 2100  
 Los Angeles, California 90036  
 (323) 934-2300 voice  
 (323) 934-0202 facsimile  
[reastham@ladas.com](mailto:reastham@ladas.com)

Enclosures: supplemental declaration with exhibits A, B, and C  
return Receipt Postcard

IN THE UNITED STATES PATENT AND TRADEMARK OFFICE



Applicant: Peter D. BREWER ) Examiner: Thanhha S. Pham  
)  
Serial No.: 10/787,276 ) Art Unit: 2813  
)  
Filed: February 25, 2004 ) Our Ref: B-4712 620052-7  
)  
For: "SELF-MASKING DEFECT ) Date: May 3, 2007  
REMOVING METHOD" )

SUPPLEMENTAL DECLARATION OF PETER D. BREWER

PURSUANT TO 37 C.F.R. § 1.131 OR, IN THE ALTERNATIVE, 37 C.F.R. § 1.132

Mail Stop Amendment  
Commissioner for Patents  
P.O. Box 1450  
Alexandria, VA 22313-1450a

I, Peter D. Brewer, declare and say:

1. I am the inventor named in the above-identified application.
2. I refer to and incorporate by reference my earlier declaration pursuant to 37 C.F.R. 1.131 executed on September 5, 2006 and filed in the above-identified application. That earlier declaration stated that I had completed the invention disclosed and claimed in the above-identified application in the United States of America no later than November 8, 2001. This supplemental declaration further explains the invention that was completed no later than November 8, 2001. In addition, this supplemental

declaration updates the declaration executed on September 5, 2006 in reference to the amendment to claim 1 presented in the response filed with this supplemental declaration.

3. As noted in the declaration executed on September 5, 2006, Exhibit A to that declaration was a copy of a "Progress, Status and Management Report" for research on "Antimonide Based Compound Semiconductors (ABCS)" that I helped to prepare. The date of the report was stated on its cover: November 8, 2001. Irrelevant material was been redacted from the copy of the report attached as Exhibit A. The report evidenced actual reduction to practice of the invention claimed in this application before November 8, 2001.

4. The "Description of Progress" on page two of the "Progress, Status and Management Report" attached as Exhibit A to the declaration executed on September 5, 2006 contained a section that I wrote. It described research directed to a "substrate transfer technology focused on the preparation of the MBE grown epi-layer surfaces prior to wafer bonding and processes for selectively removing GaSb substrates after wafer bonding." "Morphological growth-defects on the surface of the Sb-based epilayers" are identified as problems because these defects "interfere with the bonding of the GaSb epilayers and the sapphire substrates." The solution was "a self-masking process for removing growth defects form the surface of the MBE grown Sb-based epilayers."

5. As stated in the "Progress, Status and Management Report" attached as Exhibit A to the declaration executed on September 5, 2006, the "self-masking process"

involves four processing steps: "1) coating the surface of the wafer with a thick photoresist layer (5-10 microns), 2) dry-etching the resist layer to a thickness of ~0.5 microns (to reveal the tops of the defect structures but protecting the remainder of the semiconductor surface), 3) wet chemical etching of the exposed defect structures, and 4) stripping of the remaining photoresist layer."

6. The "Progress, Status and Management Report" attached as Exhibit A observed that "this process effectively removes the protruding defect structures from the surface of the semiconductor wafer without [affecting] the surrounding epilayer material." The "Report" noted the successful results of the process: "[i]nitial results using this process to prepare as-grown HBT wafers for bonding to sapphire substrates indicate enhanced bonding yields as a result of eliminating the morphological growth defects. In these experiments, bonding surface area yields as high as 94% were obtained."

7. The step of "1) coating the surface of the wafer with a thick photoresist layer (5-10 microns)" will inherently result in the formation of a layer of photoresist on the surface of the wafer that will have a planar surface on its top surface, that is, the surface not in contact with the wafer. The reason for this is the thick photoresist will be planarized by its own surface tension and viscosity. The defects will not affect the planarity of the surface of the photoresist layer because the layer is much thicker than the defects. Note that the second step is "2) dry-etching the resist layer to a thickness of ~0.5 microns (to reveal the tops of the defect structures but protecting the remainder of the semiconductor surface)," which indicates that the defect structures will have heights

above the general surface of the wafer of no more than about one-tenth to one twentieth of the thickness of the thick photoresist layer.

8. I attach as Exhibits B and C to this supplemental declaration copies, respectively, of two articles: Jun-Bo Yoon, et al., *Planarization and Trench Filing on Sever Surface Topography with Thick Photoresist for MEMS*, SPIE Vol. 3511 (September 1998), at pp. 297-306 ("Yoon, et al.") and Peter C. Sukanek, *A Model for Spin Coating with Topography*, 136 (No. 10) J. Electrochemical Soc. 3019-3026 (October 1989)("Sukanek").

9. Yoon, et al. (Exhibit B) shows that to achieve a value of planarity ( $\beta$ ) greater than 95% (0.95) the value of the thickness of the photoresist ( $d_0$ ) relative to the topography of the surface ( $t_0$ ) the value of  $d_0/t_0$  must be greater than about six (6) for AZ4562 photoresist. See Figure 6(b) of Yoon, et al. at p. 303. The defect structures discussed in my Exhibit A have heights of between one and ten microns. Persons of skill in the art will understand that typical defects are crystallographic defects (also known as oval defects) and will have a height of about one micron and that defects with a greater height are only occasionally observed and are easily located and removed by known processes. Six times the height of the typical defect is 6.0 microns. A "thick photoresist layer (5-10 microns)" therefore will have good planarity. The planarity will be greater than 90%.

10. Sukanek (Exhibit B) discusses some of the physical factors that result in greater planarity as a result of using thick photoresist films. Sukanek assumes (at page 3020, item h) that the characteristic height of the substrate variations  $\alpha_p$  (that is, the topography of the defects on the surface) is much less than L (the thickness of the

photoresist). Sukanek states in his abstract that the "viscosity and surface tension of the film [of photoresist], together with their variation with solvent content, play an important role in determining whether planar or conformal surfaces are achieved. Surface tension tends to planarize the film, whereas surface tension gradients tend to make the film more conformal. If viscosity rises very quickly as a result of solvent evaporation, the film topography becomes 'frozen-in,' and surface forces cannot planarize." This behavior is described mathematically in equation 39 on page 3022 and is described in words in the paragraph below it: "[f]rom this result, it is seen that a planar surface ( $y_{ns}=0$ ) is achieved . . . when the surface tension is very large."

11. Accordingly, a person of skill would know that the step of "1) coating the surface of the wafer with a thick photoresist layer (5-10 microns)" would inherently result in the formation of a layer of photoresist on the surface of the wafer that will have a planar surface on the top surface of the photoresist

12. I understand that claim 1 of this application is being amended to read as follows:

A method for removing defects from a semiconductor surface,  
comprising:

coating the semiconductor surface and the defects with a protective  
layer, wherein the protective layer has a planar top surface;

thinning the protective layer to selectively reveal top portions of  
the defects;

removing the defects; and

removing the protective layer.

U. S. Appl'n. No. 10/787,276  
Supplemental Declaration of Peter D. Brewer

Page 6

This method is disclosed in Exhibit A, the "Progress, Status and Management Report." The "protective layer" reads on the "thick photoresist layer," which as mentioned above, inherently had a planar top surface because of its own surface tension and viscosity.

I declare further that all statements made herein of my own knowledge are true; that all statements made herein on information and belief are believed to be true; and further that these statements were made with the knowledge that willful false statements and the like are punishable by fine or imprisonment, or both, under Section 1001 of Title 18 of the United States Code and that such willful false statements may jeopardize the validity of this application or any patents issuing thereon.

Date: May 3, 2007



---

Peter D. Brewer

# **EXHIBIT**

**A**





3011 Malibu Canyon Road  
Malibu CA 90265

## **Progress, Status And Management Report**

**N660001-01-C-8033**

**CDRL A001**

**Antimonide Based Compound Semiconductors (ABCS)**

November 8, 2001

Period Covered: October 1 2001 –November 1, 2001

Unclassified

**SPAWAR Systems Center, San Diego**

### **Description of progress**

Work included establishing a wafer transfer process, and improvement of the performance of existing prototype ABCS-based HEMT and HBT devices.

#### **Substrate Development:**

The development of the substrate transfer technology focused on the preparation of the MBE grown epi-layer surfaces prior to wafer bonding and processes for selectively removing GaSb substrates after wafer bonding.

As reported in the previous progress report, morphological growth-defects on the surface of the Sb-based epilayers are found to interfere with the bonding of the GaSb epilayers and the sapphire substrates. The growth-defects and other particles found on the wafer surfaces, cause the bonding wafers to deform around them forming circularly un-bonded interface areas or voids. The un-bonded areas resulting from even small protuberances are fairly large, for example, a particle of ~1 micron diameter leads to an un-bonded area with a diameter of ~0.5 cm for GaSb and sapphire wafers. The defects are produced during the MBE growth of epilayers and are the result of effusion cell spitting or growth defects caused by impurities or surface imperfections on the original GaSb substrate wafer. The defects are an integral part of the semiconductor wafer surface and cannot be removed with conventional particulate removal processes. The density of defects on the wafer range from 1-100/cm<sup>2</sup> and range in size from 1-50 microns with heights typically from 1-10 microns.

HRL has developed a self-masking process for removing growth-defects from the surface of the MBE grown Sb-based epilayers. This process involves four processing steps: 1) coating the surface of the wafer with a thick photoresist layer (5-10 microns), 2) dry etching the resist layer to a thickness of ~0.5 microns (to reveal the tops of the defect structures but protecting the remainder of the semiconductor surface), 3) wet chemical etching of the exposed defect structures, and 4) stripping of the remaining photoresist layer. Although simple, this process effectively removes the protruding defect structures from the surface of the semiconductor wafer without effect the surrounding epilayer material. Initial results using this process to prepare as-grown HBT wafers for bonding to sapphire substrates indicate enhanced bonding yields as a result of eliminating the morphological growth-defects. In these experiments, bonding surface area yields as high as 94% were obtained.

A second area of this task focused on developing a process for selectively removing GaSb substrates from InAs epilayers after wafer bonding. This month's activity has centered on developing a three-step process to thin and selectively remove the GaSb substrate. The process includes the following steps: 1) lap and polish the GaSb substrate (bonded to sapphire) to a thickness of 50 microns, 2) continue thinning of the GaSb substrate material to ~20 microns using a selective wet chemical etch, and 3) remove thinned GaSb material from the InAs epilayers using a highly selective dry etch process. The multi-step process is used to efficiently remove the substrate material from the epilayer device structure and not over burden the dry etch system with excessively long etch runs. The dry etch process uses an inductively coupled plasma etch system using a Cl-based etch chemistry that has demonstrated etch selectivity of 1000:1 for GaSb and InAs, respectively. This process was successfully used to completely remove the GaSb substrate material from a InAs diode structure epilayer bonded to sapphire.

**EXHIBIT**  
**B**

# Planarization and trench filling on severe surface topography with thick photoresist for MEMS

Jun-Bo Yoon, Gilbert Y. Oh, Chul-Hi Han, Euisik Yoon, and Choong-Ki Kim

Department of Electrical Engineering, KAIST,  
373-1 Kusong-dong, Yusong-gu, Taejon 305-701, Korea

## ABSTRACT

We have examined a simple and low-cost method to achieve planarization and trench filling on a severe surface topography for MEMS. The method simply uses a single-layer coating of a thick photoresist or polyimide, where the coating thickness is much greater than the severe surface topography.

From extensive experiments, we extracted simple empirical formulae for the planarization factor  $\beta$  of the thick photoresist AZ4562 and polyimide PI2611, which let us know the minimum film thickness required to obtain a certain  $\beta$  on a given surface step height and pattern density. We could compare the planarization capability of AZ4562 and PI2611 by this method.

Moreover, after the planarization with a thick photoresist, we have shown a new way, other than the plasma etching, to remove the upper photoresist layer conformally. Therefore, we could remain the photoresist only in trenches and fill up very deep and wide trenches with the photoresist. Also, we have shown the etch-back result of PI2611 using conventional  $O_2$  plasma RIE.

Using these methods, we obtained the  $\beta$  of 98% on the surface of 20 $\mu$ m-deep and 200 $\mu$ m-wide lines and spaces with a single-coated 70 $\mu$ m-thick photoresist. And 10 $\mu$ m-deep and 200 $\mu$ m-wide trenches as well as 2 $\mu$ m-deep and 50 $\mu$ m-wide trenches were neatly filled up with the photoresist. As applications for MEMS, We fabricated microchannels by metal coating after the trench fill-up process, and even multilevel microchannels by controlling the height of the photoresist remaining in the trench and repeating the trench fill-up process.

**Keywords:** Planarization, etch back, trench fill, thick photoresist, polyimide, microchannel, MEMS, planarization factor

## 1. INTRODUCTION

Planarization is the term that becomes more and more important along with advances in IC technology in the ULSI era and emerging MEMS. As an example, multilevel metallization introduces recent Chemical Mechanical Polishing (CMP) for global planarization in VLSI application.<sup>1</sup> For MEMS, the topography of the substrate is increasingly modified: bulk micromachining etches the substrate, surface micromachining usually deposit sacrificial layer and high-aspect-ratio microstructures on the surface. Once the surface of the substrate has severe nonplanarity, usually no more process can be possible due to the limited depth of focus of the exposure optics in projection aligner and gap between mask and wafer in contact aligner.

There are many techniques for planarizing surface with topography, mainly three methods: sacrificial layer and etch-back (EB),<sup>2</sup> in other words, plasma planarization,<sup>3</sup> selective dielectric deposition (SDD),<sup>4</sup> and CMP.<sup>1</sup> In SDD, surface condition can easily affect the dielectric deposition, and for CMP, global planarization can be possible, however, the method suffers from a dishing effect, surface scratch, and residual contamination.

---

Further author information –

J.-B. Yoon (correspondence): Email: jbyoon@eeinfo.kaist.ac.kr; WWW: <http://mirine.kaist.ac.kr>; Telephone: +82-42-869-8524; Fax: +82-42-869-8530

C.-H. Han: Email: [chhan@eeikaist.kaist.ac.kr](mailto:chhan@eeikaist.kaist.ac.kr); WWW: <http://mirine.kaist.ac.kr>; Telephone: +82-42-869-3444

E. Yoon: Email: [esyoon@eeikaist.kaist.ac.kr](mailto:esyoon@eeikaist.kaist.ac.kr); WWW: <http://iml.kaist.ac.kr>; Telephone: +82-42-869-3462

In EB, a low viscosity sacrificial layer (usually photoresist or polyimide) is used to spin-coat the uneven substrate surface to obtain a flat surface. Subsequently, plasma etching is used to etch-back the sacrificial layer with equal etch rate with the substrate as shown in Figure 1. Because it is simple and cost-effective, many types of approaches have been studying for EB: two or multi-layer planarization (TLP or MLP),<sup>2, 5-7</sup> image reversal and coating (IRC),<sup>8-9</sup> defocused resist patterning with blanket stripe mask (DRESS),<sup>10</sup> and planarization block mask (PBM).<sup>11</sup> These need additional lithographic steps or photomasks, or suffer from interactions between multiple polymers. By the way, planarization with single polymer layer was attempted,<sup>12</sup> however, the thickness of the sacrificial polymer layer was limited about one micrometer in that time, so that the degree of the planarization was not good.

In this paper, our key idea is very simple that applying the film much thicker than the surface topography. Therefore, we have approached the single-layer planarization with thick photoresist and polyimide. Using single or multiple coatings of the same photoresist with thickness over 100 $\mu\text{m}$ , if necessary, we have shown successful planarization results on the surface with severe topography for MEMS as well as IC applications. And from extensive experiments, we have extracted a simple empirical model, which let us know the minimum film thickness required to obtain a certain planarization level on a given surface step and pattern density.

Moreover, after the planarization, we have experimented an easy way to remove conformally the upper photoresist layer to remain the photoresist only in trenches, and hence to fill up very deep and wide trenches with the photoresist. Also, a plasma etch-back experiment for polyimide has been shown.

As an application of this technique, we have fabricated microchannels by metal coating after the trench fill-up process, and even multilevel microchannels by controlling the height of the photoresist remaining in the trench and repeating the trench fill-up process.

## 2. PLANARIZATION WITH THICK PHOTORESIST

### 2.1 THICK PHOTORESIST AZ4562 AND POLYIMIDE PI2611

Thick photoresist AZ4562, the thickest one in AZ4000 series manufactured by Hoechst, is a Novolac type, highly viscous (400cSt), and highly transparent photoresist. It has been frequently used for MEMS applications: TAB/bump process,<sup>13</sup> high-aspect-ratio photolithography,<sup>14</sup> and 3D UV-microforming.<sup>15</sup> Mainly, this photoresist is used as a high-aspect-ratio mold for electroplating.

To obtain the relationship between the film thickness and the spin speed as well as the spin time, we coated the photoresist on 4-inch wafers by a conventional spin coater and measured the film thickness. Figure 2 shows the result. Figure 2(a), which was presented by the vendor, shows the film thickness,  $d_0$ , is proportional to the inverse square root of the spin rpm, and Figure 2(b), which was own experimented, also shows the film thickness is proportional to the inverse square root of the spin time.

We obtained the film thickness over 10 $\mu\text{m}$  by reducing the spin time, not by reducing the spin speed, as the vendor recommended for the film uniformity. For the film thickness uniformity, 1 $\mu\text{m}$  standard deviation in 50 $\mu\text{m}$  film thickness<sup>16</sup> and uniformity variation with the spin speed was reported elsewhere.<sup>15</sup> In our experiment, uniformity of  $\pm 5\%$  for single coating of the 90 $\mu\text{m}$ -thick photoresist over a 4-inch wafer was observed excluding the thick edge bead. For thicker films, multiple coating is effective. No interaction was observed between layers with a sufficient soft baking, which is consistent with the fact of double thickness with double coatings.<sup>9</sup>

For the supplementary and comparison purpose, polyimide PI2611, manufactured by DuPont, has also been used. Figure 3 shows the relationship between the film thickness and the spin speed as well as the spin time of PI2611.

### 2.2 EXPERIMENTS

#### 2.2.1 DEFINITION OF THE PLANARIZATION FACTOR $\beta$

Prior to describing the experiment procedure, the term *planarization factor*  $\beta$  needs to be defined as it pertains to our work. As shown in Figure 4(a), the definition of the planarization factor  $\beta$  is given by,<sup>17</sup>

$$\beta = 1 - \frac{t_{step}^f}{t_{step}^i}, \quad (1)$$

where  $t_{step}^i$  and  $t_{step}^f$  are the initial and final step heights, respectively. In complete planarization cases,  $\beta=1$ ; if no planarization exists, then  $\beta=0$ . And according to Figure 4(b), our  $\beta$  can be expressed as,

$$\beta = 1 - \frac{(d2 + t0) - d1}{d1} = \frac{2d1 - d2 - t0}{d1}, \quad (2)$$

where  $t0$ ,  $d1$ , and  $d2$  are the surface step height, film thickness in the groove, and film thickness on the mesa, respectively.

## 2.2.2 TEST VEHICLE PREPARATION

For making surface steps with vertical cross-section, we used anisotropic etching of (110) surface-oriented silicon wafer. The surface step height varied from 2 $\mu\text{m}$  up to 20 $\mu\text{m}$ , and pattern density from 5 $\mu\text{m}$  lines & spaces (L&S) up to 200 $\mu\text{m}$  L&S. The L&S pattern had 5000 $\mu\text{m}$  in length. The KOH-etched wafer was RCA-cleaned and HMDS vapor-primed for photoresist coating. We fixed the spin speed to 2000 rpm and varied the spin time to obtain the film thickness from 10 $\mu\text{m}$  up to 100 $\mu\text{m}$ . For the film thickness over 40 $\mu\text{m}$ , we used multiple coating. After all the single coating of the photoresist, the air stabilization for 20min is followed by the soft baking at 90°C for 20min on a hot plate.

For polyimide PI2611, L&S patterns were fabricated on the flat wafer by electroplating copper up to 10 $\mu\text{m}$  thick with the same photomask used for the silicon etching. Over the copper L&S pattern, PI2611 was coated at 2000rpm with various times, then soft-cured in convection oven with  $\text{N}_2$  ambient at 200°C for 30min followed by hard curing at 300°C for 30min in the same environment.

## 2.2.3 THICKNESS MEASUREMENT

Samples are cleaved and all thickness parameters are obtained from viewing the cross-section by the ruler-armed optical microscope. The cleaved plane is (111) plane, and is perpendicular to the (110) wafer surface. For PI2611, the surface profile was measured using  $\alpha$ -step manufactured by Tencor.

## 2.3 PLANARIZATION RESULTS

Figure 5(a) shows the 20 $\mu\text{m}$ -depth step with 200 $\mu\text{m}$  L&S, which was planarized by 70 $\mu\text{m}$ -thick photoresist to have a  $\beta$  of 98%. And Figure 5(b) is for the 20 $\mu\text{m}$ -depth step with 20 $\mu\text{m}$  lines and 90 $\mu\text{m}$  spaces, which was planarized by 23 $\mu\text{m}$ -thick photoresist to have a  $\beta$  of 93%. The Figure 5(c) was obtained after applying 30 $\mu\text{m}$ -thick PI2611 on 9.5 $\mu\text{m}$ -thick copper patterns of 100 $\mu\text{m}$  L&S, and  $t_{step}^f$  of only 1 $\mu\text{m}$  was observed ( $\beta=96\%$ ).

## 2.4 EMPIRICAL FORMULA FOR $\beta$

We extensively experimented for planarization by applying films of various thickness on various surface topography. The planarization factor  $\beta$  was surely affected by the step height, pattern density, and film thickness. There already has been an empirical model for calculating  $d1$ , the photoresist thickness over space as given by,<sup>18</sup>

$$d1 = d0 + \int_0^{\infty} \int_0^{\pi} h(r, \theta) f(r/s) r d\theta dr, \quad (4)$$

where  $h(r, \theta)$  is the actual height of the surface topography;  $r$  and  $\theta$  are the cylindrical coordinates,  $f$  is a monotonically decreasing weighting function of  $r$  and  $s$ , e.g.,  $\exp(-r/s)$ , with  $s$  being the characteristic length of the material.

However, we needed a more easy and practical formula to know the minimum film thickness required to obtain a certain  $\beta$  on a given step height and pattern density. We tried to extract an empirical formula for  $\beta$  using an experimental result that when  $d0$  and  $d2$  were normalized to the surface step height ( $d0/t0$ ,  $d2/t0$ ), many experiments showed linear relationships between  $d0/t0$  and  $d2/t0$ .<sup>19</sup> They just used the result for observing photoresist step coverage, however, we used it for

estimating the  $\beta$ . And we observed that the normalized  $d1$  also showed linear relationships with  $d0/t0$  as shown in Figure 6(a), where the data were extracted from the 200 $\mu\text{m}$  L&S pattern with 2~20 $\mu\text{m}$  step and 10~100 $\mu\text{m}$  film thickness. From the linear fitting parameters, the formula for  $\beta$  can be expressed as,

$$\text{If, } \frac{d1}{t0} = a1 \frac{d0}{t0} + b1 \text{ and } \frac{d2}{t0} = a2 \frac{d0}{t0} + b2,$$

$$\beta = \frac{2\left(\frac{d1}{t0}\right) - \left(\frac{d2}{t0}\right) - \left(\frac{t0}{t0}\right)}{\frac{d1}{t0}} = \frac{(2a1 - a2) \frac{d0}{t0} + 2b1 - b2 - 1}{a1 \frac{d0}{t0} + b1}, \quad (3)$$

where  $a1$ ,  $b1$ ,  $a2$ , and  $b2$  are the linear fitting parameters. Therefore, from several test measurements, we can extract the parameters for a given pattern density, and then, we can have an empirical formula for  $\beta$  with a function of only  $d0/t0$ .

Figure 6 shows the linear fitting parameters, empirical formulae, and measured  $\beta$  of AZ4562 for the L&S of 200 $\mu\text{m}/200\mu\text{m}$ . And Figure 7 shows the similar results for PI2611. From Figure 6 and 7, we can see the linearity is well observed. In Figure 8, we can see the relationship between  $\beta$  and pattern density, and we can compare the planarization capability of AZ4562 and PI2611.

From these empirical formulae for  $\beta$ , we can estimate how much thick the applying film should be to planarize 10 $\mu\text{m}$ -thick 300 $\mu\text{m}$  lines and 100 $\mu\text{m}$  spaces with the  $\beta$  of 80%. The answer can be easily obtained from Figure 8 that a 20 $\mu\text{m}$ -thick film of AZ4562 or 40 $\mu\text{m}$ -thick film of PI2611 will be more than enough, because the 200 $\mu\text{m}$  L&S data covers the case of 300 $\mu\text{m}$  lines and 100 $\mu\text{m}$  spaces.

### 3. TRENCH FILL UP WITH THICK PHOTORESIST

In addition to planarization, we investigated etch-back methods. For thick photoresist AZ4562, we tried a new method, not the conventional gas-phase plasma etching, that is Underexposure and Overdevelopment Technique (UOT). Figure 9 illustrates this simple concept. Once the surface is planarized by the thick photoresist, the photoresist is to be exposed with no photomask and insufficient exposure dose. Then the development is to be proceeded until only the trench is filled up with the photoresist. Figure 10 shows the development rate is notably decreased as the development proceeds, when the exposure dose is not sufficient, therefore, the remaining thickness is well controlled by the exposure dose. Also, UOT can be repeated several times to etch very thick film, and used to pre-etch the thick film to a certain thickness level that is affordable to the following plasma etching step.

We obtained several results on the trench filling as shown in Figure 11. The V-grooves in Figure 11(a) has the depth of 15 $\mu\text{m}$ , the trench in Figure 11(b) has the width and depth of 200 $\mu\text{m}$  and 10 $\mu\text{m}$ , respectively, and the trench in Figure 11(c) has the width and depth of 50 $\mu\text{m}$  and 2.3 $\mu\text{m}$ , respectively.

After the trench filling, metal layer can be vacuum-deposited (and electroplated, if thicker layer is preferable), then the photoresist is removed to make microchannels for MEMS. Figure 12(a) shows 40 $\mu\text{m}$ -wide, 2.3 $\mu\text{m}$ -deep microchannels. And Figure 12(b) shows 10 $\mu\text{m}$ -wide, 2.3 $\mu\text{m}$ -deep, and 5 $\mu\text{m}$ -separated microchannels that are corresponding to 1693dpi nozzles for an inkjet printhead. Also, Figure 12(c) shows 6 $\mu\text{m}$ -wide, 7.8 $\mu\text{m}$ -deep, and 4 $\mu\text{m}$ -separated microchannels that are corresponding to 2540dpi nozzles. Also we fabricated multilevel microchannels by repeating UOT and metal deposition along with controlling photoresist depth in the trench during UOT, and the fabricated two-lever microchannels are given in Figure 13.

In addition to UOT, we applied the conventional plasma etching to etch-back of PI2611. We used the Reactive Ion Etching (RIE) with the condition of 100W, 150mTorr, and 20sccm  $\text{O}_2$ . The etching rate of PI2611 was 0.34 $\mu\text{m}/\text{min}$ . We etched the sample of Figure 6, which was 30 $\mu\text{m}$ -thick PI2611 on 9.5 $\mu\text{m}$ -thick copper patterns of 100 $\mu\text{m}$  L&S, and obtained the surface profile as shown in Figure 14(a) after 40min etching. We got Figure 14(b) just after the etch front met the copper, we stopped etching when we observed the appearance of copper by the viewing port in the RIE. Figure 14 together with Figure 6 shows that the planarized surface profile was maintained during the RIE.

#### 4. SUMMARY

In this work, we applied thick photoresist and polyimide to planarization and trench filling on a severe surface topography for MEMS. The 10–100 $\mu\text{m}$ -thick film was tried to planarize surface steps of up to 20 $\mu\text{m}$ -deep and 200 $\mu\text{m}$ -wide L&S.

From the empirical formula of the planarization factor, we could estimate the minimum film thickness that is required to obtain a certain planarization factor on a given surface step and pattern density. And we could compare the planarization capability of the photoresist AZ4562 and the polyimide PI2611 by this formula.

Also, we could fill severe trenches with the photoresist by a new simple method, UOT after the planarization. For etch-back of the polyimide, we used the conventional plasma etching with  $\text{O}_2$  plasma RIE and observed good preservation of the surface profile.

These methods are very simple, therefore cost-effective, and adequate to planarize and fill the severe surface topography usually occurred in MEMS. As applications for MEMS, We fabricated microchannels and even multilevel microchannels by metal coating after the trench fill-up process followed by removing the photoresist. We showed microchannels corresponding to 2540dpi nozzles for an inkjet printhead. This technique is expected to be easily applied to other microfluidic device fabrication as well as ultra-high density inkjet printheads.

#### 5. REFERENCES

1. William J. Patrick et al., "Application of Chemical Mechanical Polishing to the Fabrication of VLSI Circuit Interconnections," *J. Electrochem. Soc.*, vol. 138, pp. 1778-1784, 1991.
2. A. Schiltz and M. Pons, "Two-layer planarization process," *J. Electrochem. Soc.*, vol. 133, pp. 178-181, 1986.
3. A. C. Adams, "Plasma planarization," *Solid State Technology*, vol. 24, no. 4, pp. 178-181, 1981.
4. C. Y. Ting et al., "Study of planarized sputter-deposited  $\text{SiO}_2$ ," *J. Vac. Technol.*, vol. 15, p. 1105, 1978.
5. S. Crapella and F. Gualandris, "Planarization by Two-Resist Level," *J. Electrochem. Soc.*, vol. 135, pp. 683-685, 1988.
6. E. Bassous et al., "A Three-Layer Resist System for Deep U.V. and RIE Microlithography on Nonplanar Surfaces," *J. Electrochem. Soc.*, vol. 130, pp. 478-484, 1983.
7. T. T. Pampalone et al., "Novolac Resin Planarization Layers for Multilayer Resist Imaging Systems," *J. Electrochem. Soc.*, vol. 133, pp. 2394-2398, 1986.
8. Gordon Grivna and Ray Goodner, "A New Global Planarization Technique Using *In Situ* Isotropic Photoresist Mask Erosion," *J. Electrochem. Soc.*, vol. 141, pp. 251-254, 1994.
9. Yuan Xiong Li et al., "Plasma Planarization for Sensor Applications," *IEEE J. of MEMS*, Vol. 4, pp. 132-138, Sep. 1995.
10. Y. Matsubara et al., "A Novel Global Planarization Technology using Defocused Resist Patterning with Blanket Stripe Mask (DRESS)," in *Tech. Digest, IEEE Int. Electron Devices Meeting (IEDM)*, 1993, pp. 665-668.
11. T. H. Daubenspeck et al., "Planarization of ULSI Topography over Variable Pattern Densities," *J. Electrochem. Soc.*, vol. 138, pp. 506-509, 1991.
12. L. K. White, "Planarization Properties of Resist and Polyimide Coatings," *J. Electrochem. Soc.*, vol. 130, pp. 1543-1548, 1983.
13. E. Cullmann et al., "3D structures for micro-system technology using proximity lithography," *Solid State Tech.*, pp. 93-96, March 1995.
14. H. Miyajima and M. Mehregany, "High-Aspect-Ratio Photolithography for MEMS applications," *IEEE J. of MEMS*, vol. 4, no. 4, pp. 220-229, Dec. 1995.
15. B. Loechel and A. Maciossek, "Surface micro components fabricated by UV depth lithography and electroplating," *Proc. of SPIE*, vol. 2639, pp. 174-184, 1995.
16. Application Note in Suss Report, vol. 9, qu. 3, p. 12 (1995).
17. S. Wolf, *Silicon Processing for the VLSI Era*, vol. 2, pp. 201. Lattice Press, 1990.
18. R. H. Wilson and P. A. Piacente, "Effect of Circuit Structure on Planarization Resist Thickness," *J. Electrochem. Soc.*, vol. 133, pp. 981-984, 1986.
19. K. Hirata et al., "Dry Etching Technology for 1-  $\mu\text{m}$  VLSI Fabrication," *IEEE Trans. Electron Devices*, vol. ED-28, pp. 1323-1331, Nov. 1981.



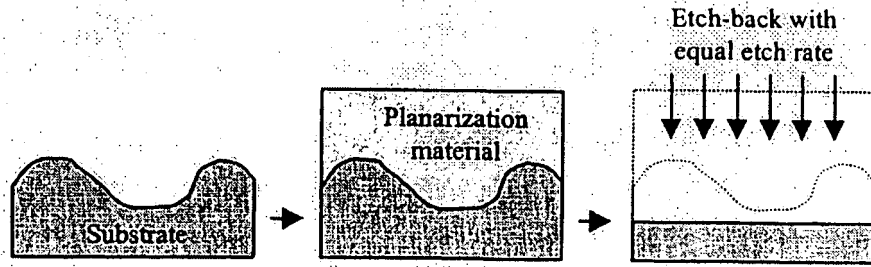


Figure 1. Planarization by sacrificial layer and etch-back.

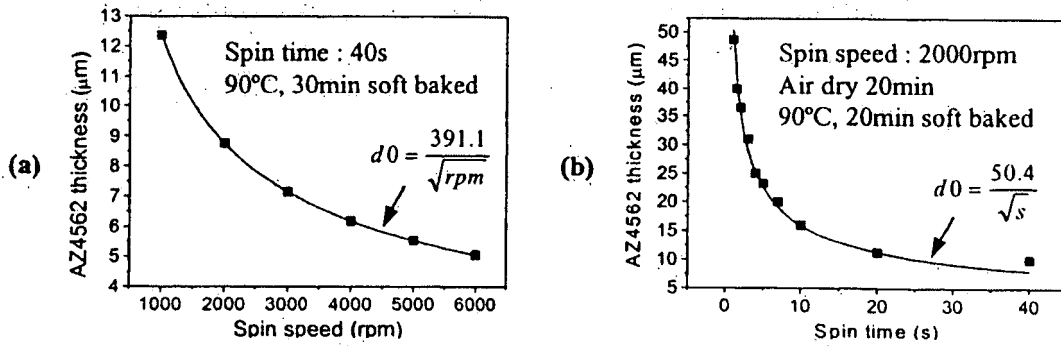


Figure 2. The film thickness of AZ4562 with coating conditions. (a) Spin speed vs. film thickness (b) Spin time vs. film thickness

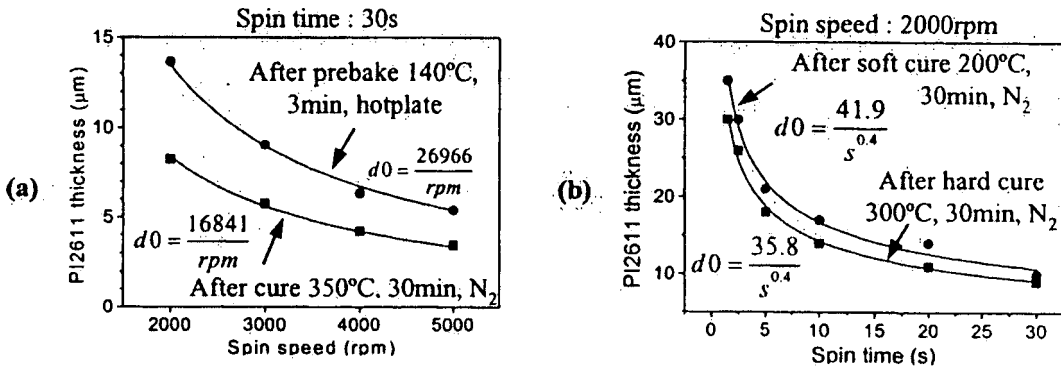


Figure 3. The film thickness of PI2611 with coating conditions. (a) Spin speed vs. film thickness (b) Spin time vs. film thickness

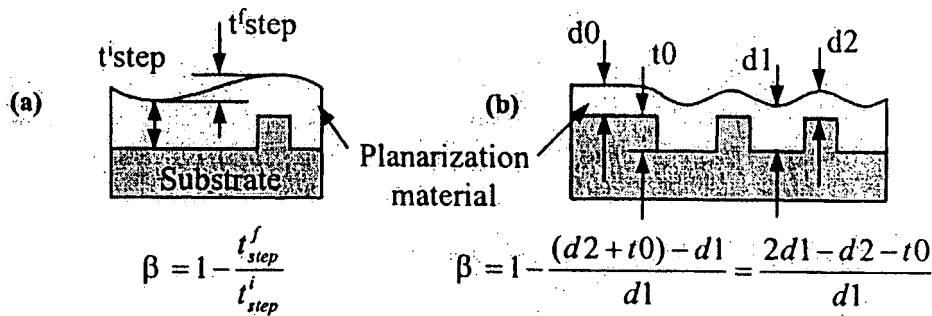


Figure 4. The definition of the planarization factor  $\beta$ . (a) From the reference<sup>17</sup> (b) In this work

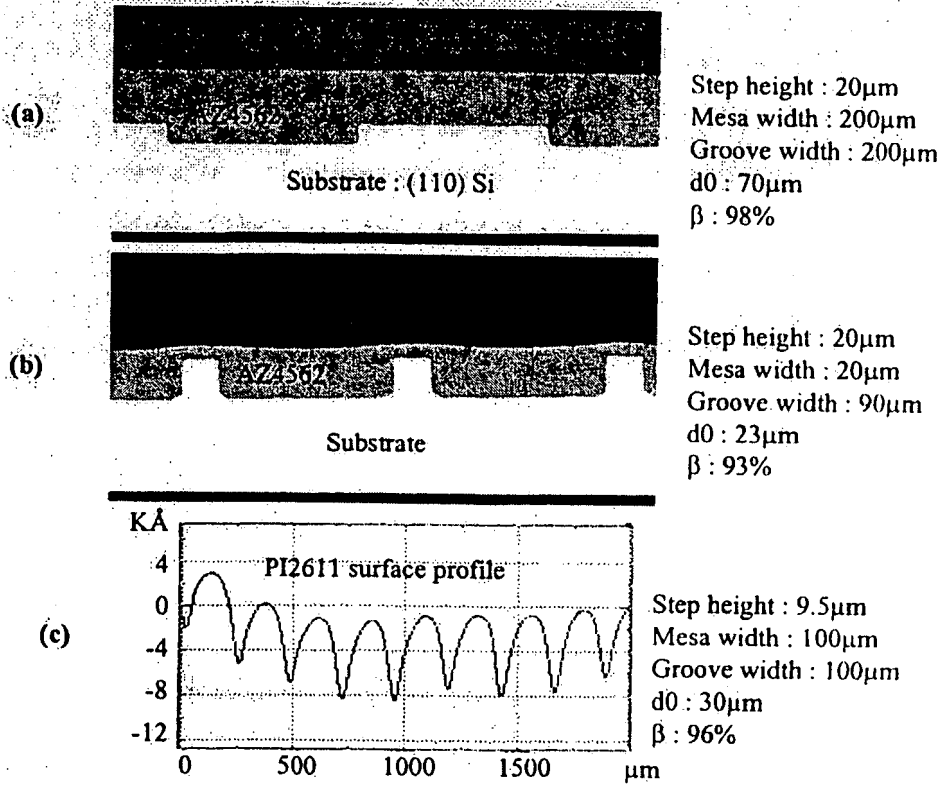


Figure 5. Planarization results. (a), (b) Cross-sectional view (c) Surface profile by  $\alpha$ -step (Tencor)

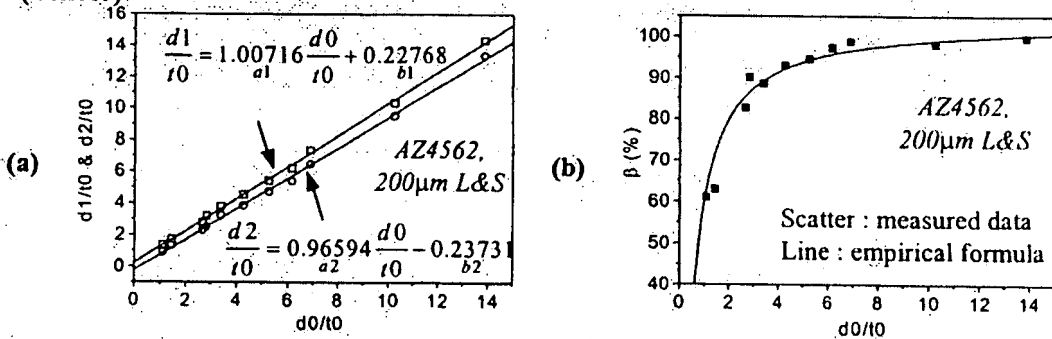


Figure 6. An empirical formula for  $\beta$  from the linear relationships between  $d1/t0$  and  $d0/t0$ ,  $d2/t0$  and  $d0/t0$ . (a) Linear parameters extraction (b) Obtained empirical formula

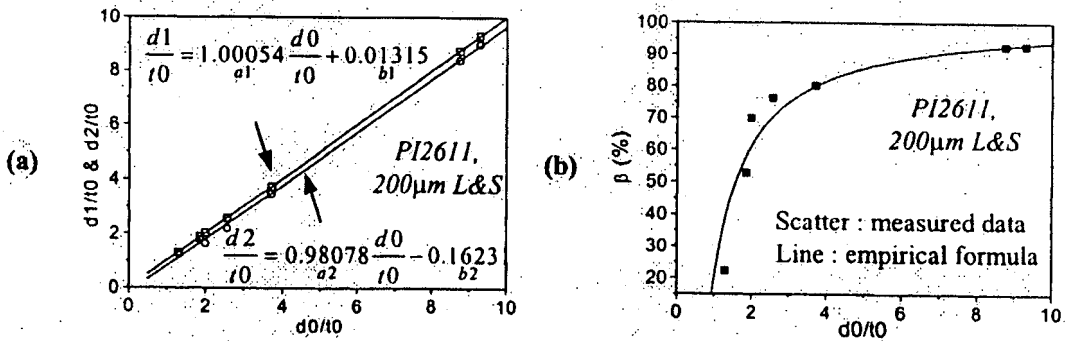


Figure 7. An empirical formula for  $\beta$  of PI2611, 200 $\mu$ m L&S. (a) Linear parameters extraction (b) Obtained empirical formula

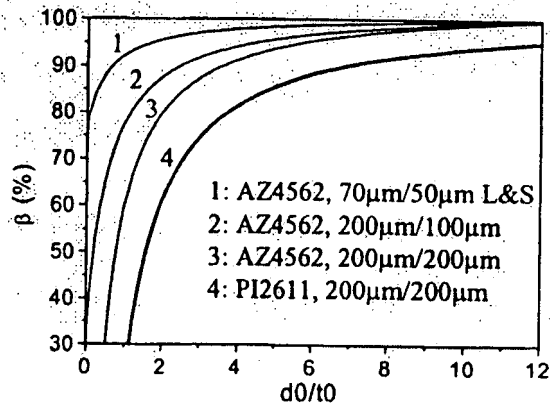


Figure 8. Comparison of the planarization factor  $\beta$  by empirical formulae.

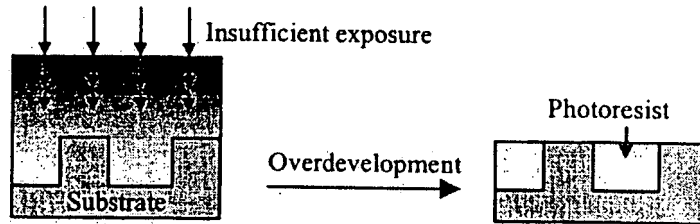


Figure 9. Underexposure and Overdevelopment Technique (UOT).

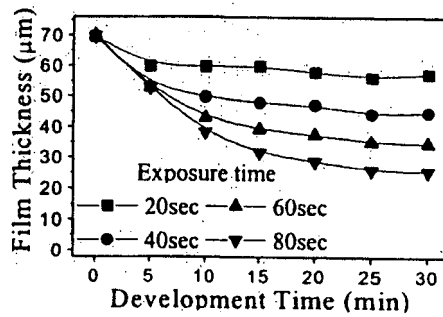


Figure 10. The overdevelopment characteristic with varying the exposure time.

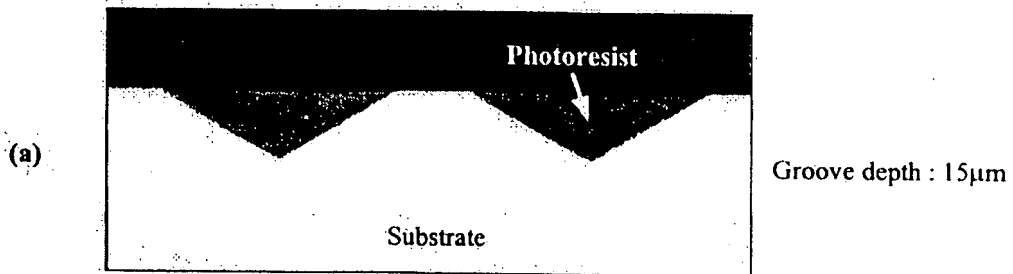


Figure 11. Several results on the trench filling with thick photoresist by UOT. (a) Cross-sectional view of the V-groove

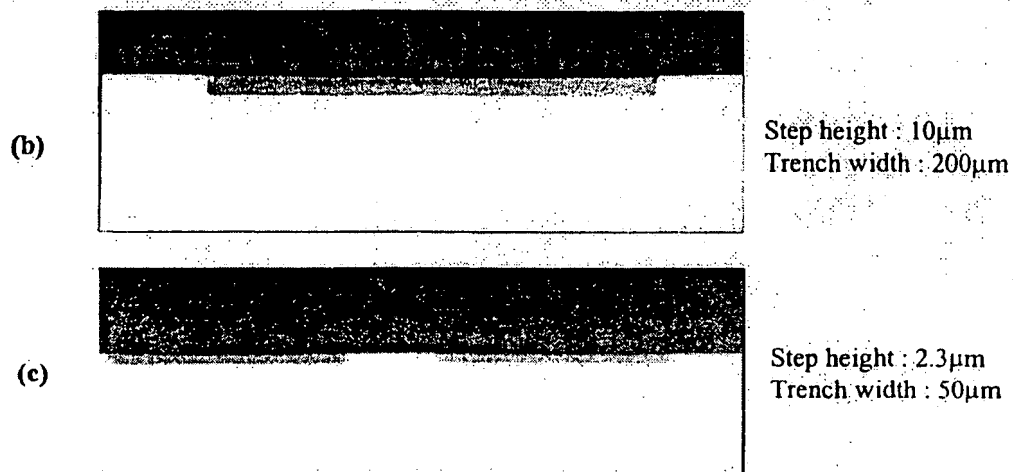


Figure 11. (continued) (b) the deep and wide trench (c) the shallow and wide trench

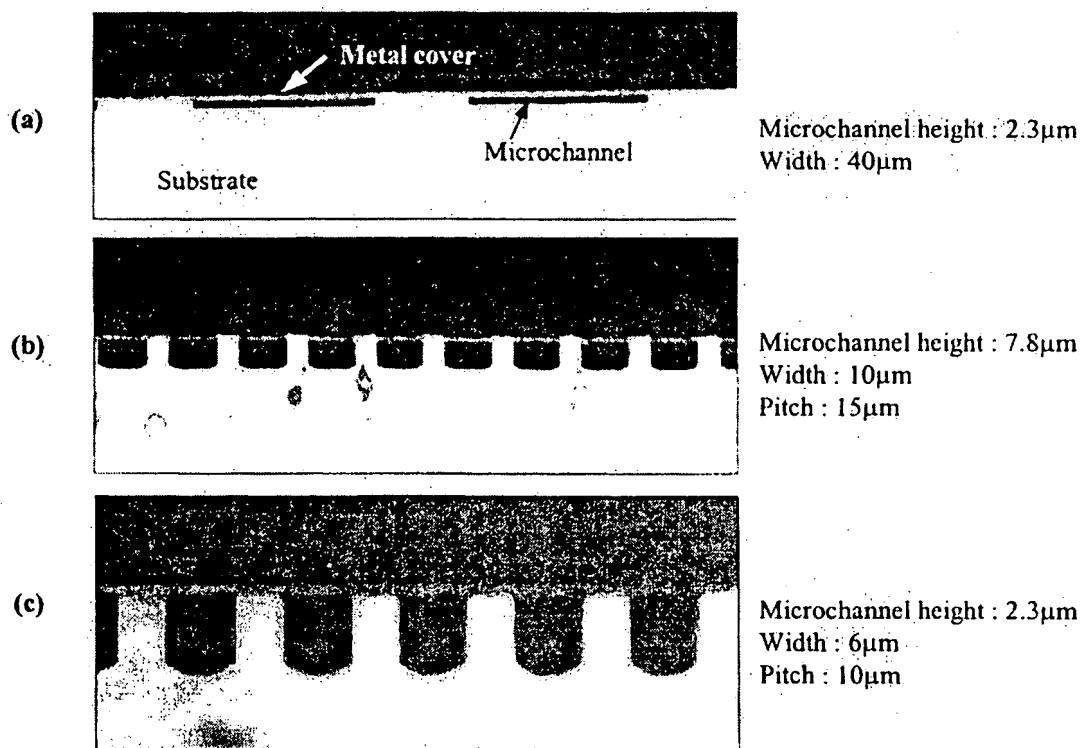


Figure 12. Microchannels made by UOT and metal deposition. (a) Cross-sectional view of the shallow and wide microchannels (b) Corresponding to 1693dpi (dots per inch) nozzles for an inkjet printhead (c) Corresponding to 2540dpi nozzles

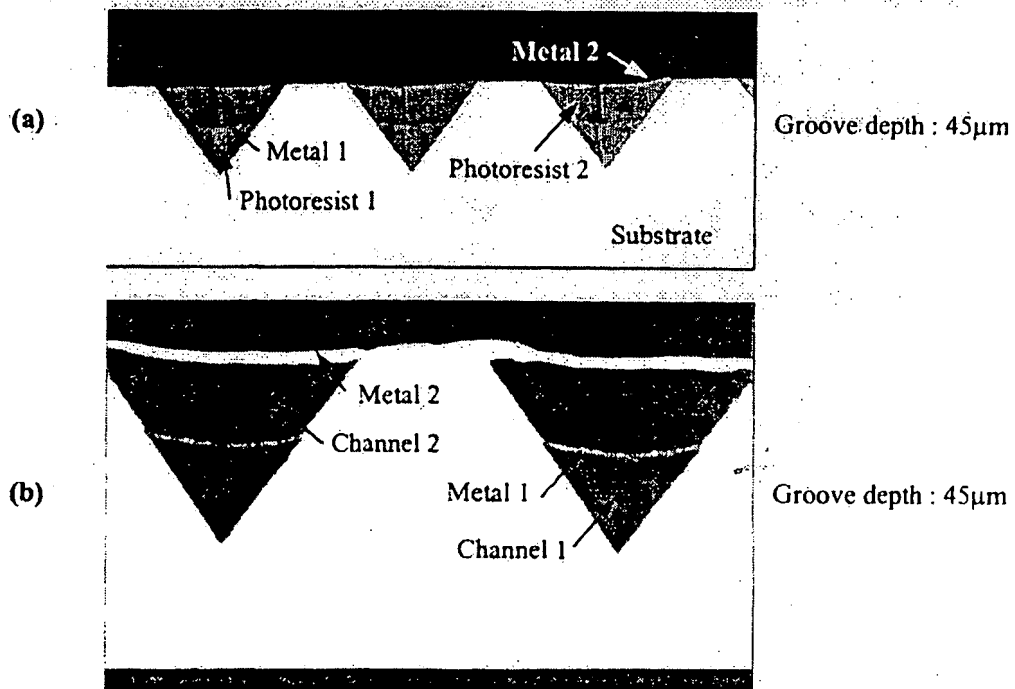


Figure 13. Multilevel microchannels made by repeating UOT and metal deposition. (a) Cross-sectional view of the two-level microchannels before removing the photoresist (b) Magnified view of them after removing the photoresist

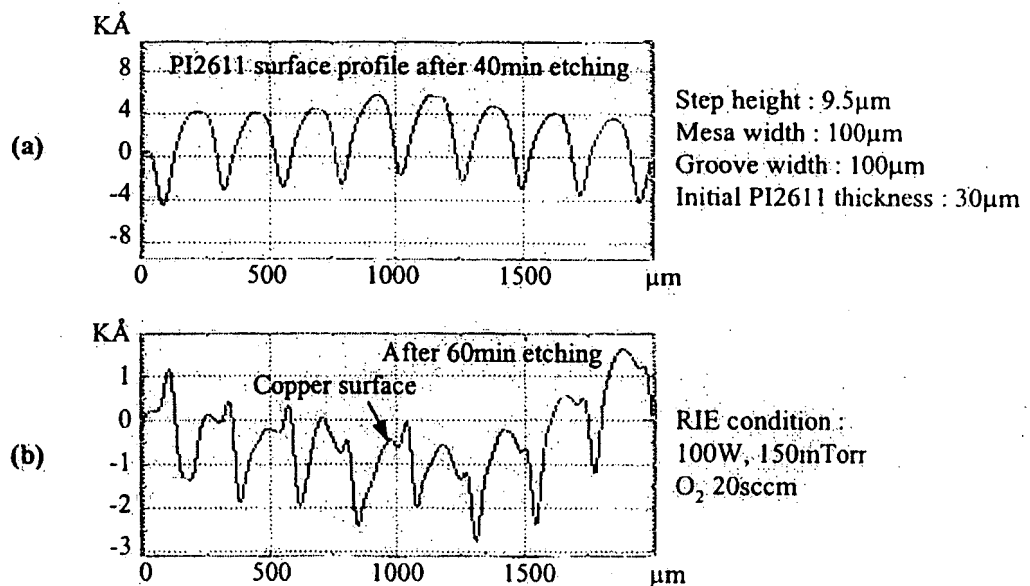


Figure 14. The result of the conventional plasma etch-back of PI2611 used in Figure 6. The surface profile was measured by Tencor's  $\alpha$ -step (a) After 40min etching (b) After finishing the etch-back

**EXHIBIT**  
**C**

# A Model for Spin Coating with Topography

Peter C. Sukanek\*,<sup>1</sup>

Philips Research Laboratories, 5600 JA Eindhoven, The Netherlands

## ABSTRACT

A theoretical model for spin coating on a substrate with topography is presented. The equations assume a thin film, with uniform properties in the direction normal to the substrate. By assuming a small amplitude for the substrate variations, two sets of coupled equations are derived, one for the mean value of the thickness and its composition, and another for the fluctuations. The viscosity and surface tension of the film, together with their variation with solvent content, play an important role in determining whether planar or conformal surfaces are achieved. Surface tension tends to planarize the film, whereas surface tension gradients tend to make the film more conformal. If viscosity rises very quickly as a result of solvent evaporation, the film topography becomes "frozen-in," and surface forces cannot planarize.

Spin coating is widely used in the microelectronics industry to produce thin, uniform coatings of materials from solution on substrates. The most common type of material is an organic photoresist, which is then used in a lithographic operation to delineate patterns. In many applications, the substrate on which the resist is spun is not uniform, but processes some variation in height as a result of previous processing. The relation between the topography of the substrate and that of the resulting film is important.

In most applications, it is desirable to achieve a planar resist surface, regardless of the extent of underlying height variations. This is the case, for example, in lithography with a small depth of focus, where slight variations in the distance of the resist film from the optical system would adversely affect the quality of the latent image. A planar film is also required in etch-back metallization. In this process, a metal layer is formed with "pillars," and then covered with a conformal dielectric. A planar resist film is then applied, and etched in such a way that the resist and dielectric are removed at the same rate. At the end of the process, all that remains are the metal pillars protruding from the dielectric. These then form the contacts for the second layer metal.

In other applications, however, it may be advantageous to achieve a conformal film. This is the case for the dielectric discussed above, which could be spun onto the substrate as a polyimide or spin-on glass. In lithography with a large depth of focus, conformal coverage would not compromise the image quality and may reduce the necessity of over-developing the pattern in some areas.

In a series of publications, White (1-5) has described an empirical model for coating on topography. The substrate surface is expressed as a Fourier series. The coating surface is assumed to be of the same form, but with different Fourier coefficients. These coefficients are determined by applying a low pass frequency filter to the substrate coefficients. The filter is assumed to be characterized by two empirical parameters which must be determined for each different photoresist and for different operating conditions, such as the spin speed and post-apply bake temperature.

A different, but related, approach was taken by Wilson and Piacente (6, 7). These authors define an "average structure height" in terms of an undefined function of position on the surface. This function is different for different types of resists and different processing methods. While the authors do not do so, the function can apparently be determined empirically by measuring the resist height on wafers with different types of topography.

Stillwagon *et al.* (8) take a more fundamental view of the leveling process. These authors derive an expression for the "leveling time," the time required for a non-evaporating film to planarize as a result of a surface tension-driven flow. The film is assumed to be conformal after the coating process, and then flow during a leveling period. In their experiments, liquid epoxies were used, which were then cured, and the resulting topography measured. Their

"model" was meant to indicate the relative effect of important variables such as mean thickness, viscosity, surface tension, and feature size.

While the empirical approaches mentioned above appear to be successful, it would be advantageous to have a model available which relates the film topography to the physical properties of the resist as well as the coating and post-apply conditions. For use with photoresists, solvent evaporation effects should be included, as well as the variation of surface tension and viscosity with the solvent content. Previously, a model was developed for spin coating on flat substrates (9). The model predictions are in good agreement, at least qualitatively, with available data. It predicts, for example, that the film height increases with the initial solids fraction, the initial viscosity of the solution and with the solvent volatility, and that it is inversely proportional to the square root of the spin speed. In this paper, the model is extended to predict the variation of thickness on a substrate with small, periodic height variations.

The model draws on earlier work by Overdiep on the leveling of paints (10-11). In many ways, the problems are similar. Overdiep shows that the coating surface over a rough substrate depends on the surface tension of the coating material and how the tension varies with composition during the drying process. In Overdiep's model, which assumes a constant evaporation rate during the drying, either a planar or a conformal coating can be achieved depending upon whether surface tension or surface tension gradient effects dominate the process. The predictions of the present model agree qualitatively with those results. However, there are differences. In particular, substrate rotation must be accounted for in the present analysis. In addition, a decreasing evaporation rate is included in the present model, as is a more complete description of the normal stress condition at the film surface.

## Theoretical

A complete solution to the problem would be quite complicated. In the present treatment, a number of assumptions are employed. The major ones are as follows:

- The time scale for the thinning,  $t'$ , is much larger than that for the rotational flow,  $\Omega$ . Hence, for the equations used here, the rotational flow appears only as the driving force for the radial velocity.
- The characteristic length for the film thickness,  $L$ , is much smaller than the substrate radius,  $R$ . Consequently, the lubrication approximation may be employed.
- The fluid has two components, a volatile solvent and a nonvolatile solute.
- The process is isothermal.
- The film is uniform throughout its thickness. Hence, it may be characterized by a single value of the solvent fraction,  $x$ , which may only depend on time and the radial and azimuthal coordinates,  $r$  and  $\theta$ .
- Solvent evaporation may be modeled as mass transfer from a rotating disk. The mass transfer coefficient is constant over the surface, and increases as the square root of the spin speed.

\* Electrochemical Society Active Member.

<sup>1</sup> Present address: Department of Chemical Engineering, Clarkson University, Potsdam, New York 13676.

g) The viscosity of the fluid depends on the liquid fraction, but is independent of the shear rate.

h) The characteristic height of the substrate variations,  $a_p$ , is much less than  $L$ .

i) The substrate is periodic in  $r$  and  $\theta$ .

A critique of assumptions a) through g) is provided by Bornside *et al.* (12). The most restrictive assumption is probably e). As solvent diffuses from the film, the diffusivity of the material drops, making further evaporation more difficult. This would cause axial gradients in the film, which are ignored here.

Previously (9), the complete equations of conservation of mass and momentum were put into dimensionless form and simplified with assumption b). While a similar approach could be employed here, it is simpler to make the standard lubrication approximations (13) at the outset. In addition to the radial flow driven by the rotation of the substrate, surface tension effects at the film-air interface drive an azimuthal flow, as well as affecting the radial flow.

The simplified radial and azimuthal components of the equation of conservation of momentum are (symbols are defined in the List of Symbols section)

$$-\rho r \Omega^2 = -\frac{\partial p}{\partial r} + \mu \frac{\partial^2 v_z}{\partial z^2} \quad [1]$$

$$0 = -\frac{1}{r} \frac{\partial p}{\partial \theta} + \mu \frac{\partial^2 v_\theta}{\partial z^2} \quad [2]$$

The fluid is assumed to adhere to the substrate at the surface,  $z_0$ . At the top of the film,  $z = h$ , the stresses are balanced by surface tension variations

$$z = z_0: v_r = 0 \quad [3]$$

$$v_\theta = 0$$

$$z = h: \mu \frac{\partial v_r}{\partial z} = \frac{\partial \sigma}{\partial r} \quad [4]$$

$$\mu \frac{\partial v_\theta}{\partial z} = \frac{1}{r} \frac{\partial \sigma}{\partial \theta}$$

These equations are easily solved for the velocity profiles and the flow rates (per unit circumference) in the radial and azimuthal directions. These are given by

$$v_r = \frac{z - z_0}{\mu} \left\{ \left( \rho r \Omega^2 - \frac{\partial p}{\partial r} \right) \left( h - \frac{z + z_0}{2} \right) + \frac{\partial \sigma}{\partial r} \right\} \quad [5]$$

$$v_\theta = \frac{z - z_0}{r \mu} \left\{ -\frac{\partial p}{\partial \theta} \left( h - \frac{z + z_0}{2} \right) + \frac{\partial \sigma}{\partial \theta} \right\} \quad [6]$$

$$q_r = \left( \rho r \Omega^2 - \frac{\partial p}{\partial r} \right) \frac{(h - z_0)^3}{3\mu} + \frac{\partial \sigma}{\partial r} \frac{(h - z_0)^2}{2\mu} \quad [7]$$

$$q_\theta = -\frac{1}{r} \frac{\partial p}{\partial \theta} \frac{(h - z_0)^3}{3\mu} + \frac{1}{r} \frac{\partial \sigma}{\partial \theta} \frac{(h - z_0)^2}{2\mu} \quad [8]$$

Total and species mass balances on a differential area of the film give the following equations for film thickness and solvent fraction

$$\frac{\partial h}{\partial t} = -\frac{1}{r} \frac{\partial}{\partial r} (r q_r) - \frac{1}{r} \frac{\partial}{\partial \theta} q_\theta - e/\rho \quad [9]$$

$$(h - z_0) \frac{\partial x}{\partial t} = -q_r \frac{\partial x}{\partial r} - q_\theta \frac{1}{r} \frac{\partial x}{\partial \theta} - e(1 - x)/\rho \quad [10]$$

where  $e$  is the solvent flux from the film resulting from evaporation. With assumption f), this may be written as

$$e = \rho k(x - x_R) \quad [11]$$

and  $k$  is the mass transfer coefficient, with units of velocity. For laminar mass transfer on a rotating disk (9)

$$k = \alpha \Omega^{0.5} \quad [12]$$

Included in Eq. [11] is a parameter,  $x_R$ , to account for solvent which remains in the film after processing. It is known that there is always some solvent remaining after spinning, and also after a typical post-apply bake (14). The probable physical reason for this solvent retention is the greatly reduced diffusivity through the solvent-depleted surface regions of the film, as discussed above. The film does not come to equilibrium with the atmosphere under normal processing conditions. Since the present model assumes uniform properties throughout the film [assumption e)], this effect cannot be accounted for. Thus the residual solvent must be considered an empirical quantity.

The above equations must be solved with an expression for the pressure. This is given by a balance between pressure, viscous and surface tension forces at the film-air interface

$$-p + 2\mu \frac{\partial v_z}{\partial z} = \sigma \left[ \frac{1}{r} \frac{\partial}{\partial r} \left( r \frac{\partial h}{\partial r} \right) + \frac{1}{r^2} \frac{\partial^2 h}{\partial \theta^2} \right] \quad [13]$$

It is convenient to put the defining equations into dimensionless form using the following variables

$$y = h/L \quad \eta = \mu/\mu^0 \quad \zeta = z/L \quad P = p/L/\sigma^0$$

$$\tau = t/t' \quad \gamma = \sigma/\sigma^0 \quad \xi = r/L \quad u = v_z t'/L \quad [14]$$

where  $L$  and  $t'$  are the characteristic length and time scales used previously (9)

$$L = (\alpha \mu^0/\rho)^{1/3} \Omega^{-1/2} \quad [15]$$

$$t' = (\mu^0/\rho)^{1/3} \alpha^{-2/3} \Omega^{-1}$$

The ratio  $L/t'$  is the mass transfer coefficient, a characteristic velocity for the problem. In the absence of rotation (during baking, for example), the dimensionless distance and time scales are then

$$L_B = h_B^0 \quad [16]$$

$$t'_B = h_B^0/k$$

where the subscript B is used to indicate baking conditions, and o indicates the value prior to baking.

The dimensionless equations for the film height, solvent fraction, and pressure are

$$\begin{aligned} \frac{\partial y}{\partial \tau} = \mathcal{R} \left\{ \frac{2(y - \zeta_0)^3}{3\eta} + \xi \frac{(y - \zeta_0)^2}{\eta} \frac{\partial}{\partial \xi} (y - \zeta_0) \right\} - (x - x_R) \\ + \frac{1}{\text{Ca}\eta} \left\{ \frac{(y - \zeta_0)^3}{3} \mathcal{F}P - \frac{(y - \zeta_0)^2}{2} \Gamma \mathcal{F}x \right. \\ \left. + (y - \zeta_0)^2 \left[ \frac{\partial P}{\partial \xi} \frac{\partial}{\partial \xi} (y - \zeta_0) + \frac{1}{\xi^2} \frac{\partial P}{\partial \theta} \frac{\partial}{\partial \theta} (y - \zeta_0) \right] \right. \\ \left. + \Gamma(y - \zeta_0) \left[ \frac{\partial x}{\partial \xi} \frac{\partial}{\partial \xi} (y - \zeta_0) + \frac{1}{\xi^2} \frac{\partial x}{\partial \theta} \frac{\partial}{\partial \theta} (y - \zeta_0) \right] \right\} \quad [17] \end{aligned}$$

$$\begin{aligned} \frac{\partial x}{\partial \tau} = -\mathcal{R} \frac{\xi}{3\eta} (y - \zeta_0)^2 \frac{\partial x}{\partial \xi} - \frac{(x - x_R)(1 - x)}{y - \zeta_0} \\ + \frac{1}{\text{Ca}\eta} \left\{ \frac{(y - \zeta_0)^3}{3} \left[ \frac{\partial P}{\partial \xi} \frac{\partial x}{\partial \xi} + \frac{1}{\xi^2} \frac{\partial P}{\partial \theta} \frac{\partial x}{\partial \theta} \right] \right. \\ \left. - \frac{(y - \zeta_0)^2}{2} \Gamma \left[ \left( \frac{\partial x}{\partial \xi} \right)^2 + \left( \frac{1}{\xi} \frac{\partial x}{\partial \theta} \right)^2 \right] \right\} \quad [18] \end{aligned}$$

$$-P + 2\text{Ca}\eta \frac{\partial u}{\partial \zeta} = \gamma \mathcal{F}y \quad [19]$$



where  $\Gamma$  is the variation of surface tension with solvent fraction

$$\Gamma = \frac{\partial \gamma}{\partial x} \quad [20]$$

$\mathcal{T}$  is a differential operator

$$\mathcal{T}y = \frac{1}{\xi} \frac{\partial}{\partial \xi} \left( \xi \frac{\partial y}{\partial \xi} \right) + \frac{1}{\xi^2} \frac{\partial^2 y}{\partial \theta^2} \quad [21]$$

and  $Ca$  is the capillary number, the ratio of viscous to surface tension forces

$$Ca = \mu^0 k / \sigma^0 \quad [22]$$

In these equations, a "rotation parameter,"  $\mathcal{R}$ , has been introduced. Those terms which  $\mathcal{R}$  multiplies arise because of the rotation of the substrate; the other terms arise from evaporation and surface tension effects. Hence, when the substrate rotates,  $\mathcal{R} = 1$ . In a typical spin coating operation, the film is baked after the apply step. During the bake,  $\mathcal{R}$  is 0.

The surface roughness is assumed to be of the form

$$\zeta_0 = \alpha \varphi(\xi, \theta) \quad [23]$$

In order to solve these equations, the amplitude of the surface roughness is assumed to be small. The film height  $y$ , solvent concentration  $x$ , and pressure  $P$  are expanded in a series in terms of  $\alpha$

$$y = y_0 + \alpha y_1 + \alpha^2 y_2 + \dots \quad [24]$$

$$x = x_0 + \alpha x_1 + \alpha^2 x_2 + \dots$$

$$P = P_0 + \alpha P_1 + \alpha^2 P_2 + \dots$$

The residual solvent content,  $x_R$ , is assumed to be constant.

These expressions are substituted into Eq. [17]-[19], and terms of like power in  $\alpha$  equated. At zero order (a smooth substrate), the height is assumed to be independent of position. This is in agreement with previous results for spinning on a flat substrate (9). The equations for the first two orders of  $x$  and  $y$  are

$$\frac{\partial y_0}{\partial \tau} = -\mathcal{R} \frac{2y_0^3}{3\eta} - (x_0 - x_R) \quad [25]$$

$$\frac{\partial x_0}{\partial \tau} = - \frac{(x_0 - x_R)(1 - x_0)}{y_0} \quad [26]$$

$$\frac{\partial y_1}{\partial \tau} = -\mathcal{R} \frac{y_0^2}{\eta} \left\{ \frac{1}{\xi} \frac{\partial}{\partial \xi} [\xi^2 (y_1 - \varphi)] - \frac{2}{3} \frac{y_0}{\eta} N x_1 \right\} - x_1 + \frac{1}{Ca\eta} \left\{ \frac{y_0^3}{3} \mathcal{T}P_1 - \frac{y_0^2}{2} \Gamma \mathcal{T}x_1 \right\} \quad [27]$$

$$\frac{\partial x_1}{\partial \tau} = -\mathcal{R} \frac{y_0^2}{3\eta} \frac{\partial x_1}{\partial \xi} - \frac{x_1(1 - 2x_0 + x_R)}{y_0} + \frac{(y_1 - \varphi)(x_0 - x_R)(1 - x_0)}{y_0^2} \quad [28]$$

The equation for the pressure at first order is

$$-P_1 - 2Ca \frac{y_0}{\xi} \frac{\partial}{\partial \xi} [\xi^2 (y_1 - \varphi)] + y_0^2 \mathcal{T}P_1 - 2y_0 \Gamma \mathcal{T}x_1 = -\gamma \mathcal{T}y_1 \quad [29]$$

Equations [25] and [26] are identical to those found previously (9). The parameter  $N$  is the variation of viscosity with solvent fraction

$$N = \frac{\partial \eta}{\partial x} \quad [30]$$

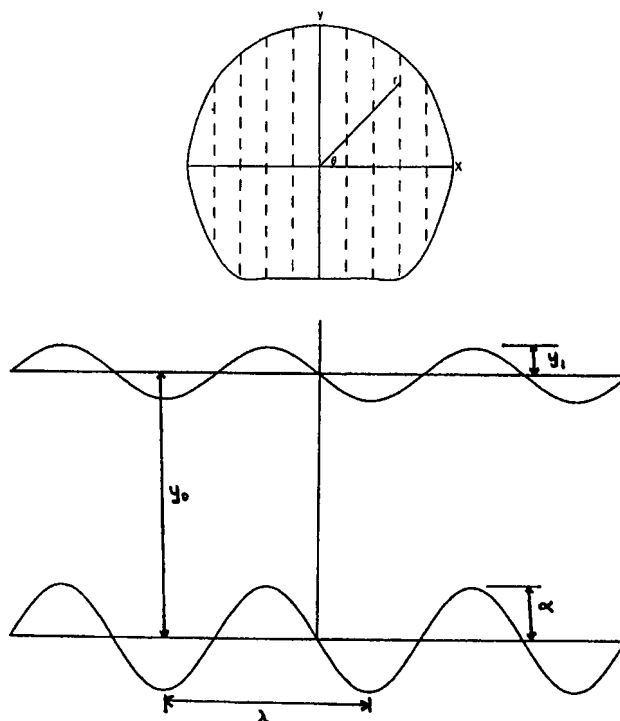


Fig. 1. Surface geometry indicating wavelength ( $\lambda$ ) and amplitude ( $\alpha$ ) of the surface roughness, the mean film height ( $y_0$ ), and the surface amplitude ( $y_1$ ). With  $y_1 = 1$ , the surface is conformal; with  $y_1 = 0$ , the surface is planar.

Before further progress can be made in solving the equations, the surface roughness must be specified. In what follows, we assume that the surface has a periodic roughness in one direction only. In this case, the most general expression for  $\varphi$  is

$$\varphi = \sum \varphi_{sn} \sin(n\Lambda \xi \cos \theta) \quad [31]$$

with  $\varphi_{s1} = 1$ . The geometry is illustrated in Fig. 1 for the case of sinusoidal variations. More complicated forms of the roughness can be easily treated by including cosine terms in the expansion. However, non-periodic structures and isolated features cannot be treated in this manner. A Fourier integral technique must be used in that case.

With this simple form, the film thickness, solvent fraction, and pressure may be assumed to depend on a single parameter,  $\chi$

$$\chi = \xi \cos \theta \quad [32]$$

The solution of these equations is assumed to be of the form

$$(y_1, x_1, P_1) = \sum (y_{ns}, x_{ns}, P_{ns}) \sin(n\Lambda \chi) \quad [33]$$

The coefficients are evaluated in the usual manner. The results is a set of coupled ordinary differential equations for the amplitude functions and pressure

$$\frac{dy_{ns}}{d\tau} = \mathcal{R} \frac{y_0^2}{\eta} \left\{ \frac{2y_0}{3\eta} N x_{ns} - \frac{3}{2} (y_{ns} - \varphi_{ns}) + \sum_{\substack{m=1 \\ m \neq n}}^{\infty} \mathcal{C}_{mn} (y_{ms} - \varphi_{ms}) - x_{ns} - \frac{1}{Ca\eta} \left\{ \frac{y_0^3}{3} (n\Lambda)^2 P_{ns} - \frac{y_0^2}{2} \Gamma (n - \Lambda)^2 x_{ns} \right\} \right\} \quad [34]$$

$$\frac{dx_{ns}}{d\tau} = \mathcal{R} \frac{y_0^2}{3\eta} \left\{ x_{ns} + \sum_{\substack{m=1 \\ m \neq n}}^{\infty} \mathcal{C}_{mn} x_{ms} \right\} - \frac{x_{ns}}{y_0} (1 - 2x_0 + x_R) + \frac{1}{y_0^2} (x_0 - x_R)(1 - x_0)(y_{ns} - \varphi_{ns}) \quad [35]$$

$$P_{ns} = \frac{\gamma(n\Lambda)^2 y_{ns} + 2y_o \Gamma(n\Lambda)^2 x_{ns} - 9Ca[3y_o(y_{ns} - \varphi_{ns}) - 2y_o \sum_{m=1}^{\infty} \epsilon_{mn}(y_{ns} - \varphi_{ns})]}{1 + (n\Lambda y_o)^2} \quad [36]$$

with

$$\epsilon_{mn} = m \left[ \frac{(-1)^{m+n}}{m+n} + \frac{(-1)^{m-n}}{m-n} \right] \quad [37]$$

Because of the rotation terms, all of the equations for the coefficients are coupled. However, as is apparent from the numerical solution, this coupling is weak, and only the first few terms must be computed.

If the capillary number is sufficiently small and the mean thickness much less than the wavelength of the topography ( $y_o \Lambda \ll 1$ ), the pressure condition, Eq. [36], reduces to

$$P_{ns} = \gamma(n\Lambda)^2 y_{ns} \quad [38]$$

This is the condition used by Overdiep (10-11).

If the capillary number were identically zero, Eq. [34] for the height fluctuation becomes an algebraic expression which can be solved to give

$$y_{ns} = \frac{x_{ns} \Gamma}{2\gamma y_o} (n - \Lambda)^2 [3 - (y_o n \Lambda)^2] \quad [39]$$

From this result, it is seen that a planar surface ( $y_{ns} = 0$ ) is achieved when the residual solvent fluctuation is zero, when the surface tension is very large ( $\gamma \rightarrow \infty$ ), or when the surface tension is independent of the composition ( $\Gamma = 0$ ). When the pitch is large compared to the thickness ( $y_o \Lambda \ll 1$ ), increasing the mean thickness or decreasing the wavelength makes the film more planar. For some conditions of topography and thickness ( $y_o \Lambda > \sqrt{3}$ ), the surface can "invert": the maximum in the film amplitude corresponds to a minimum in the substrate amplitude.

A conformal surface ( $y_{ns} = 1$ ) is obtained when there is residual solvent remaining and surface tension variations with composition are important. If there are no residual solvent fluctuations, i.e., if  $x_{ns}$  goes to zero, then the surface always becomes planar at the steady state. However, in many situations of interest, steady state for the fluctuations occurs on a much longer time scale than for the primary coating process. In addition, if the viscosity of the material approaches very large values when sufficient solvent is removed, the fluctuations may become "frozen in"

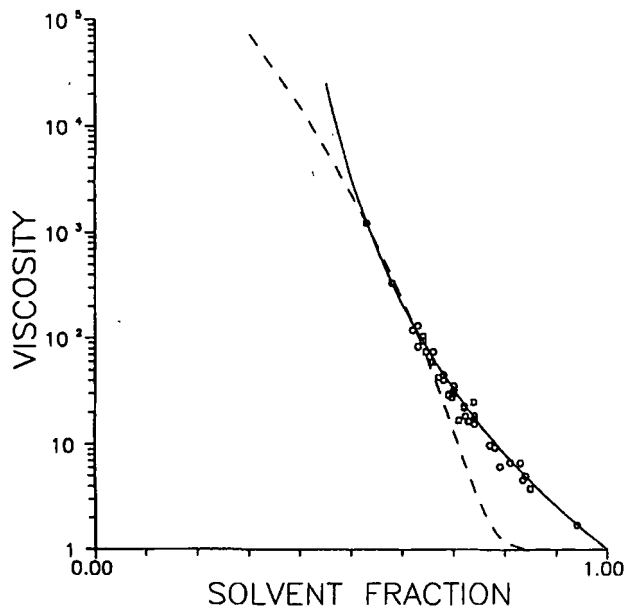


Fig. 2. Viscosity as a function of solvent fraction for a series of AZ (○) and Hunt (□) resists. Best fits of viscosity model 1 (—) and model 2 (---).

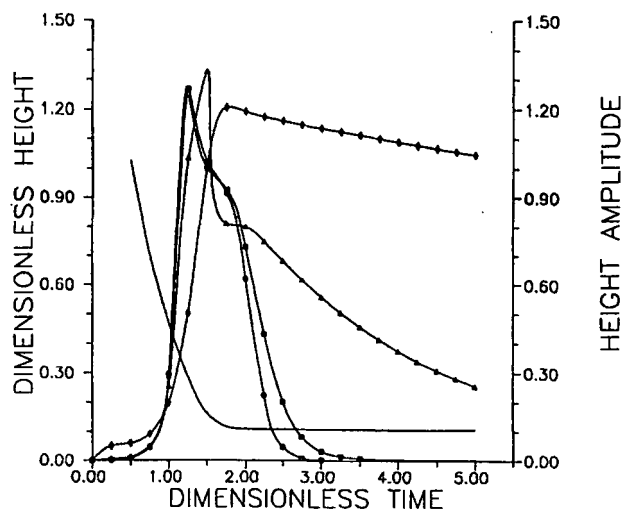


Fig. 3. Dimensionless mean height ( $y_o$ , —) and amplitude of the fluctuations ( $y_{1i}$ ) as a function of time for the base-line case with  $x_o = 1$  and  $x_h = 0$ . Capillary numbers of  $10^{-5}$  (○),  $10^{-4}$  (□),  $10^{-3}$  (△), and  $10^{-2}$  (◇).

during the spinning. In this case, the product ( $Ca \eta$ ) is finite, and Eq. [38] no longer holds. This appears to be the situation for all real films.

## Results

**Parameters.**—In order to estimate reasonable values for the various parameters needed in the solution to the equations, the characteristic length and time scale must first be found. In the calculations for the film height on a smooth substrate, the final dimensionless thickness is on the order of 0.1 (9). Since in most coating operations, the actual film thickness is approximately  $1 \mu\text{m}$ , the characteristic length scale must be on the order of  $10 \mu\text{m}$ . Likewise, the theory predicts a dimensionless time of about 3 in order to achieve a steady film thickness. The actual time found in spinning is about 30s, giving a characteristic time of about 10s. If the initial fluid viscosity is on the order of  $0.01 \text{ Pa s}$  (10 cp), and the surface tension is  $3 \times 10^{-4} \text{ kg/s}$  (30 dynes/cm), the capillary number is in the range  $10^{-4}$  to  $10^{-5}$ . For surface structures with a period of 1 to  $10 \mu\text{m}$ , the wave-number  $\Lambda$  is on the order 0.1 to 10.

Previously (9) two different viscosity models for the solution were employed. Similar models are used here as well

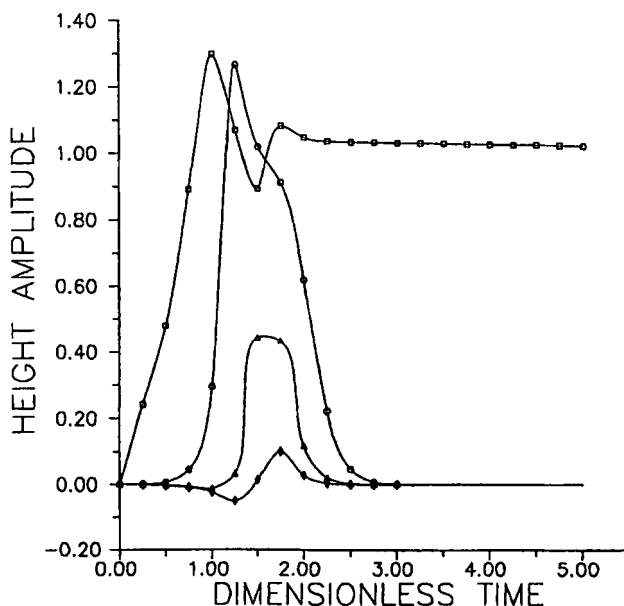


Fig. 4. Effect of substrate wave number on time dependence of the height fluctuations for the base-line case.  $\Lambda = 0.1$  (□),  $1.0$  (○),  $5.0$  (△), and  $10.0$  (◇).

Model 1:  $\eta = \{1 + [A(1 - x)]^n\} / \{1 + [A(1 - x^0)]^n\}$  [40]

Model 2:  $\eta = \{[1 - \beta(1 - x)] / [1 - \beta(1 - x^0)]\}^{n/\beta}$  [41]

Model 1 is a slight variation of the one employed previously (9).

For coating on a smooth substrate, the two models give very similar results, despite the fact that the viscosity predictions can be orders of magnitude different for small values of  $x$ . In particular, model 2 predicts infinite viscosity at a solvent fraction of  $(1 - 1/\beta)$ , called the critical solvent fraction. Presently, there is no reliable model for the viscosity over the whole range of concentrations encountered. However, Fig. 2 shows some data on standard photoresists as a function of solvent content (15). These data are clearly consistent with model 2 with a critical solvent fraction of 0.33. The results are the same for the two different manufacturers represented in the figure. This is not unreasonable since the solids and solvent are quite similar for these positive resists. Despite the better agreement with model 2, it is instructive to employ both models because of the very different types of viscosity predictions.

Likewise, there are no reliable models for surface tension variation with concentration. Photoresists usually contain surface active compounds as "leveling agents," and so may not show a linear variation. For want of a better model, we use the same variation as Eq. [40]

$\gamma = 1 + [B(1 - x)]^n / \{1 + [B(1 - x^0)]^n\}$  [42]

In addition to the physical parameters needed to solve the equations, the initial conditions are also required. Previously (9) it was found that the initial film height had no effect on the final predicted height, provided the initial value was sufficiently large (greater than about 4). For all the present calculations, an initial height of 10 was used. Numerical experiments indicated that the calculated fluctuations  $y_1$  and  $x_1$  are also insensitive to their initial values. In all the calculations presented here, zero initial fluctuations are employed.

**Model predictions.**—As a base-line case, viscosity model 1 (Eq. [40]) was used, with a value of  $A$  of 1, and an exponent of 4. The surface tension model was used with  $B = 1$  and an exponent of 2. The surface is assumed to be a simple sinusoid ( $\varphi_{2s}$ , etc. = 0). The capillary number is  $10^{-5}$ , and  $\Lambda = 1$ . Figure 3 shows the mean height,  $y_0$ , and the first Fourier coefficient of the height fluctuation (the height amplitude),  $y_{1s}$ , as a function of time with capillary number as a parameter. It is apparent that the two height values can have very different time scales. A steady mean height is achieved after a dimensionless time of about 2. However, at the time the amplitude of the surface wave indicates essentially a conformal coating for all values of the capillary number. At sufficiently long times, however, the surface is pre-

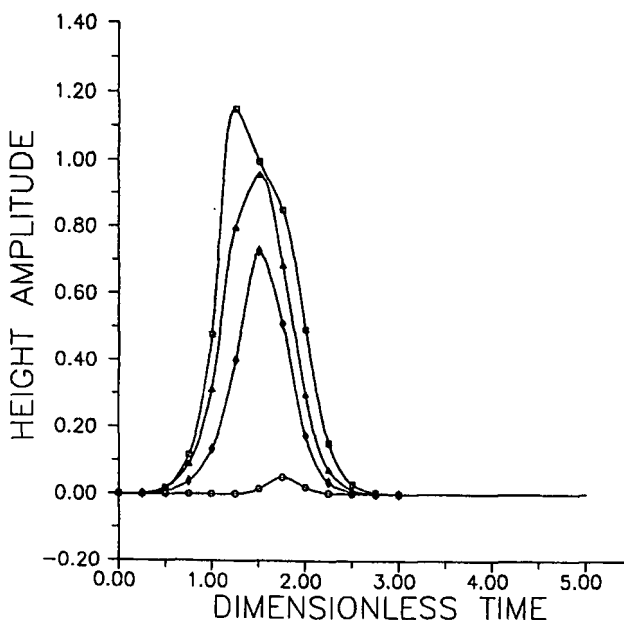


Fig. 6. Effect of surface tension gradient on the surface amplitude.  $n' = 0$  (O); 0.1 (◇), 0.3 (△), and 1.0 (□).

dicted to assume a planar value, in agreement with Eq. [39]. The time required increases as the capillary number increases. For this model, the viscosity of the fluid is always finite, so that on a very large time scale, the surface tension-driven flow can achieve planarization. The actual shape of the surface depends on all of the Fourier coefficients,  $y_{1s}$ ,  $y_{2s}$ , etc. For a sinusoidal substrate, the higher coefficients,  $y_{2s}$ , etc., are quite small, indicating an essentially sinusoidal surface.

The effect of the pitch of the topography,  $\Lambda$ , is illustrated in Fig. 4. As the pitch becomes smaller (and hence  $\Lambda$  larger), the amplitude decreases. As observed in the literature (3), the finer the structure of the surface, the more nearly planar is the coating. Figure 4 also illustrates the "inversion" predicted by Eq. [48] for the largest value of  $\Lambda$ . For all but the most widely separated features ( $\Lambda = 0.1$ ), a planar coating is predicted at long times. Figure 5 shows the effect of residual solvent. For this viscosity model, solvent remaining in the film has little effect on the type of surface which is achieved. The influence of initial solids content is also negligible. This is probably more an artifact of the viscosity model than a real result.

The influence of the surface tension gradient is shown in Fig. 6. For a constant surface tension ( $n' = 0$  in Eq. [41]), the surface is essentially always planar. However, even small variations in the surface tension with concentration

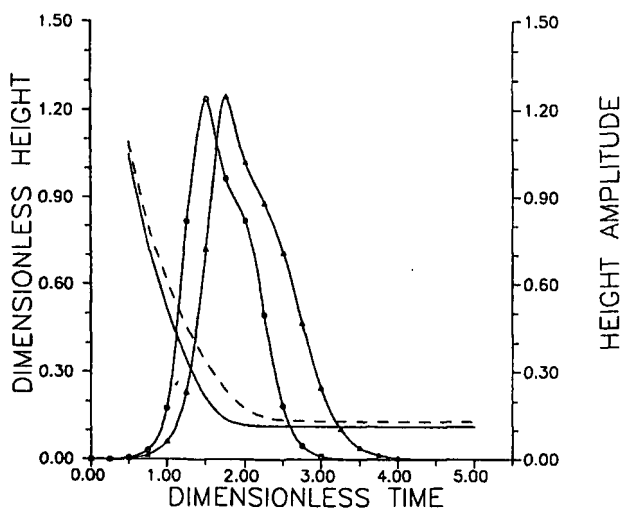


Fig. 5. Effect of residual solvent on the mean height and surface amplitude ( $y_{1s}$ ).  $x_R = 0.1$  (O; —);  $x_R = 0.3$  (△; ----). Lines without symbols refer to mean height.

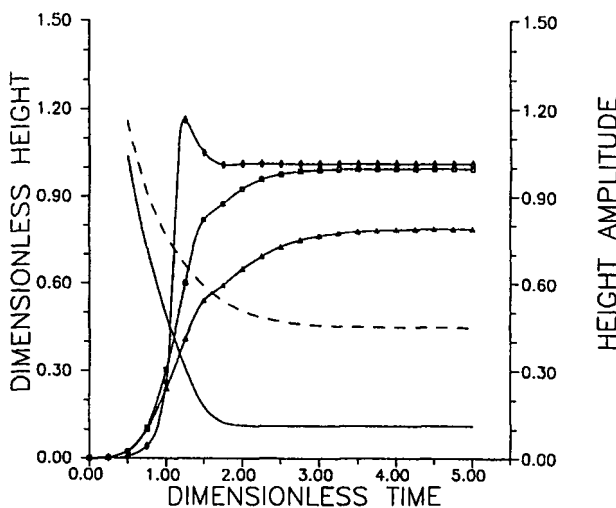


Fig. 7. Effect of initial solvent content with viscosity model 2 on mean thickness and fluctuations.  $x_0 = 0.9$  (—; ◇), 0.7 (△), and 0.6 (---; △). Lines without symbols refer to mean values.

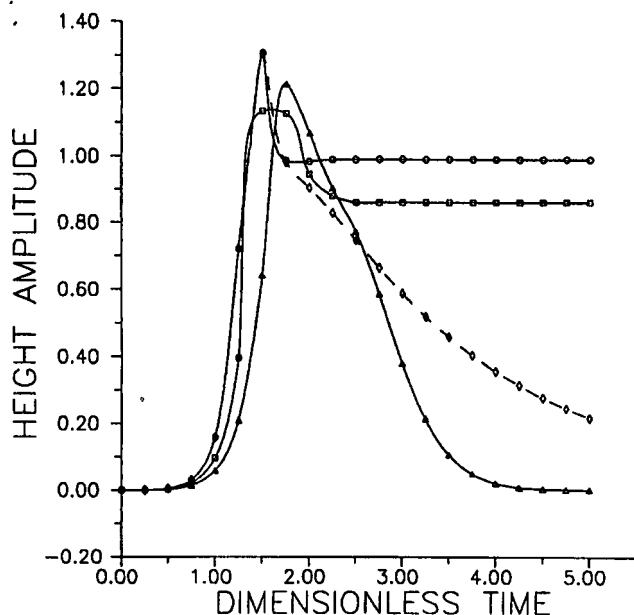


Fig. 8. Effect of residual solvent on the height fluctuations with viscosity model 2.  $x_R = 0.1$  (○), 0.2 (□), and 0.3 (△). If the viscosity remains finite during the spinning, a planar layer can be obtained. An equivalent result is found by changing the critical solvent fraction to 0.05 ( $\beta = 1.05$ ,  $x_R = 0.1$ ; ----).

can have significant effects on the magnitude of the fluctuations. This is in agreement with Eq. [38] and Overdiep's conclusion that high surface tension gradients promote a conformal surface. Figure 6 also reveals, as in the previous results, that the surface eventually planarizes at a sufficiently long time. This is due to the finite ultimate value of the viscosity.

As indicated in Fig. 2, viscosity model 2 predicts an unbounded viscosity as the solvent content reaches some critical value. Figure 7 shows the predicted mean height and surface amplitude for this model. For these calculations, a  $\beta$  value of 1.25 is used. Hence, the viscosity becomes unbounded at a solids content of 0.8. The behavior of the mean height is very similar to that predicted by model 1, as is the value of the height itself. However, if there is no residual solvent, the fluctuations become "frozen in." The viscosity becomes so large that the fluid cannot flow, preventing the film from becoming planar. Changes in the initial liquid content can modify somewhat the magnitude of the fluctuations, but a planar surface can never be achieved. In this case, increasing the initial solids content appears to reduce the fluctuations

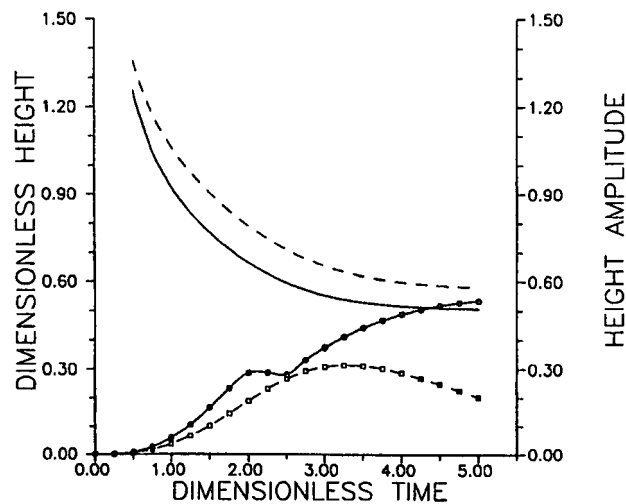


Fig. 9. Predicted mean film thickness and fluctuations for the best fit viscosity data of Fig. 2. Model 1 (—) and model 2 (----).  $x_R = 0.3$ ;  $x_0 = 0.7$ . Lines without symbols refer to mean values.

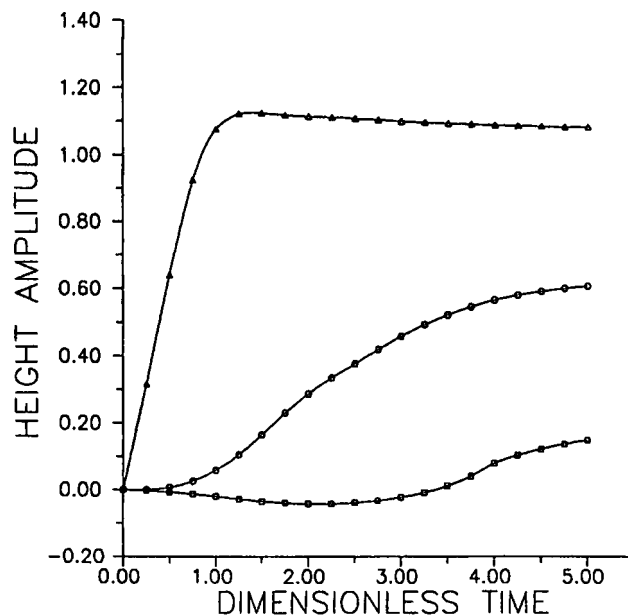


Fig. 10. First Fourier coefficient of the surface fluctuation for coverage of a step function substrate for viscosity model 2 with best fit parameters.  $x_R = 0.3$ ;  $x_0 = 0.7$ .  $\lambda = 0.1$  (△), 1.0 (○), and 5.0 (□).

because the viscosity becomes unbounded before the surface tension gradients can cause the amplitude to grow very large.

The only way to obtain a planar surface with this model is to retain more solvent in the film or to change the critical solids content. The predictions are illustrated in Fig. 8. By increasing the fraction of retained solvent from 0.1 to 0.3, planarization may be achieved using the present parameters. Similarly, if the critical solids fraction is increased to 0.95 (a  $\beta$  value of 1.05), the surface would again be planar. The values of  $x_R$  and  $\beta$  cannot be changed by altering the process parameters, however. These depend on the interactions of the polymer and solvent which make up the resist and can only be altered by changing the formulation.

The predicted profiles for a "real" resist system are shown in Fig. 9. An initial solvent fraction of 0.7 is used with a residual fraction of 0.3. Both viscosity models are employed with the "best fit" parameters from the viscosity data of Fig. 2. As expected, the mean height for the two

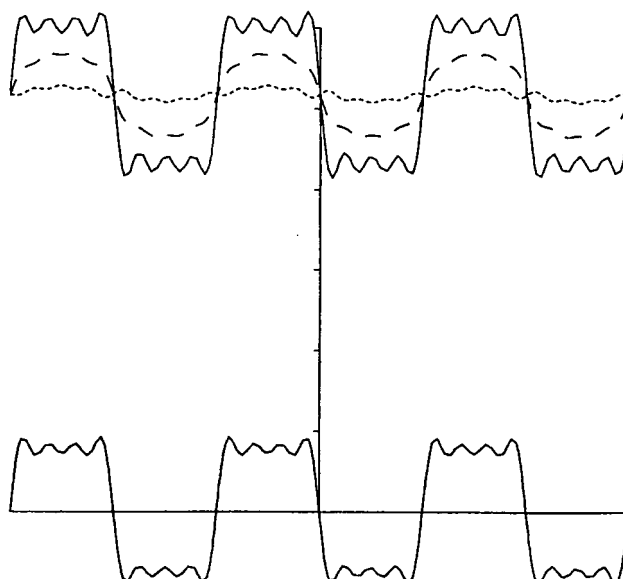


Fig. 11. The approximation of a square wave substrate with 4 terms in the series of Eq. [43] shown in the lower curve. The upper curves represent the predicted topography for model 2 viscosity function and best fit parameters for  $\lambda = 0.1$  (—), 1.0 (---) and 5.0 (.....). The dimensionless step height,  $\alpha$ , is assumed to be 0.1.

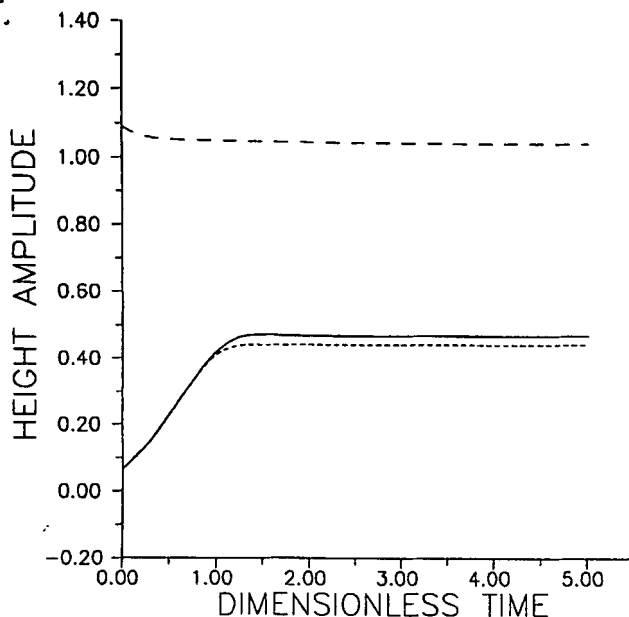


Fig. 12. Effect of post-apply bake on coating topography after two different spin procedures. In one case (— — —), the dimensionless spin time is 5, whereas in the second (— and —) this time is 1, resulting in significant retained solvent. For (— and —) the critical solids content is 0.1. For (---), it is 0.2.

models is similar, but the surface fluctuations display qualitatively different behavior. Model 1 indicates that the surface may be planarized by spinning for a sufficiently long time, while model 2 shows that the magnitude of the surface amplitude reaches some value and becomes frozen.

Thus far, the substrate has been assumed to be a sinusoid. For the more likely case of a square wave, the topography function, Eq. [31], is

$$\varphi = \sin(\Lambda\chi) + (1/3) \sin(3\Lambda\chi) + (1/5) \sin(5\Lambda\chi) + \dots \quad [43]$$

Calculations were performed using four terms in the series. Figure 10 shows the value of  $y_{1s}$ , the first term in the series for the surface, for three values of the substrate pitch and the "real" resist. With features close together (large  $\Lambda$ ), the surface tends to be more planar. When the features are far apart (small  $\Lambda$ ), the surface is conformal. Figure 11 shows the calculated actual substrate and surface topographies for the same three values of the pitch as used in Fig. 10. The first value of the substrate amplitude,  $y_{1s}$ , is seen to be a good indicator of the actual nature of the surface.

As mentioned above, the same equations, with some slight modifications, may be used to calculate the surface topography after a post-apply bake. The results of such a computation, for two different spinning times, are shown in Fig. 12. In one case, the film is spun for the full time, resulting in a high viscosity film with a low residual solvent content. In the second case, the spin time is much shorter, and the film still retains significant solvent. These predictions are based on the results for the "real" resist system. As indicated in Eq. [16] the length scale for the two problems is the film thickness after spinning. The critical solvent content at which infinite viscosity is reached is assumed to decrease to 0.1 as a result of the high temperature. This is the same as the residual solvent fraction.

The major difference between the two cases is the value of the capillary number. For the fully spun film, the viscosity will be quite high, despite the lowering somewhat by the high temperature of the bake. The value of  $Ca$  is estimated to be 0.1. The surface tension is assumed to be constant for this film. As indicated in Fig. 12, the fluctuations change only slightly during the bake. This is a result of the large capillary number. For the "wet" film, the viscosity is comparatively low. The value of  $Ca$  is taken to be  $10^{-5}$ . In this case, surface tension variations increase the value of the fluctuations to some steady value. Decreasing the

critical solids content to 0.8 reduces the surface amplitude somewhat, as shown in Fig. 12. While the theory predicts that baking a "wet" film will result in a more planar surface than when a "dry" film is used, the changes are not as dramatic as indicated in Fig. 12. This is because the length scale for the two problems is different since the initial film thicknesses are different. The actual decrease in the height amplitude as a result of partial spinning is about 15%. In this case, evaporation of the solvent from the "wet" film plays a major role in defining the film topography.

### Conclusions

A theoretical model for spin coating on topography has been developed which relates the shape of the surface to the properties of the fluid being spun, as well as to the shape of the substrate. Unlike the model for the mean thickness of the film, the surface shape is a strong function of the physical properties of the material. If the viscosity of the fluid can approach a very large value for a finite solvent fraction, the shape of the surface becomes frozen during the spinning. Planarizing the surface would require decreasing the value of this solvent fraction or increasing the amount of residual solvent in the film. In both cases, the mobility of the resist would increase. However, changing either of these values would require changes to the resist formulation. Both of these parameters must be regarded as empirical in the present formulation of the problem. The value of the critical solvent fraction is related to the chemical interaction of the solvent and the solids in the resist. The residual solvent fraction is also a result of this interaction. As such, they are outside the scope of the present fluid mechanical study.

The film surface may be "annealed" somewhat by a post-apply bake. The annealing effect is increased by spinning only a short time prior to the post-apply bake. In this way, more solvent remains in the film at the end of the spin cycle allowing more flow during the bake.

The model predicts that the surface follows the substrate for substrates which vary over large distances, and becomes planar for substrates with a short pitch. This is in agreement with available experimental data. The model is easily extended to more complex substrate geometries by expanding the substrate topography in a set of cosine as well as sine functions. In that case, an additional set of equations for the thickness and composition fluctuations must be included in the solution. The calculation for isolated features would require a different though related approach based on Fourier integrals.

In order to solve the equations, the dimensionless amplitude of the substrate topography is assumed to be "small." As is the case with all perturbation solutions, it is impossible to specify how small the neglected terms must be for the solution to be valid. If we assume  $\alpha = 0.1$ , and use a dimensionless mean height of 0.5, as indicated in Fig. 9, we can estimate a ratio of step height to film thickness ( $a_s/h$ ) of about 0.2. In many real applications, this ratio may be 0.3 to 0.5. We would expect the predictions to be qualitatively correct for these values, but the actual magnitudes of the fluctuations to be different. In particular, the conclusions regarding the effects of substrate pitch, retained solvent, critical solvent fraction, and post-apply bake should remain unaltered.

The most serious shortcoming of the model appears to be the assumption of uniform properties throughout the depth of the film. This assumption requires the inclusion of the residual solvent fraction in the model. An improved approach would include concentration variations in the film, with a concentration dependent diffusivity as well.

Manuscript submitted June 3, 1988; revised manuscript received Jan. 17, 1989.

### LIST OF SYMBOLS

A	parameter in viscosity model 1
$\alpha$	parameter in evaporation rate
B	parameter in surface tension-model
$\varphi_{mn}$	constants in equations for the amplitude functions
Ca	capillary number

$\mathcal{D}$	differential operator
$e$	evaporation rate
$h$	film thickness
$K$	equilibrium coefficient for the solvent
$k$	mass transfer coefficient
$L$	characteristic distance
$n$	exponent in viscosity model 1
$n'$	exponent in surface tension model
$N$	variation of the viscosity with composition
$P$	dimensionless pressure
$p$	pressure
$q$	flow rate
$\mathcal{R}$	rotation parameter
$r$	radial position
$t$	time
$t'$	characteristic time
$u$	dimensionless velocity in z direction
$v$	velocity
$x$	solvent fraction
$y$	dimensionless film thickness
$z$	direction normal to the substrate surface

## Greek Symbols

$\alpha$	dimensionless amplitude of surface roughness
$\beta$	parameter in viscosity model 2
$\Gamma$	variation of surface tension with composition
$\gamma$	dimensionless surface tension
$\delta$	exponent in viscosity model 2
$\eta$	dimensionless viscosity
$\Lambda$	dimensionless wavenumber of the substrate
$\chi$	position
$\theta$	azimuthal position
$\mu$	viscosity
$\rho$	density
$\xi$	dimensionless radial position
$\sigma$	surface tension
$\tau$	dimensionless time
$\varphi$	substrate topography function

$\zeta$	dimensionless position normal to substrate
$\Omega$	spin speed

## Subscripts

$B$	during post-apply bake
$R$	residual
$s$	coefficients of the sine terms in the solution
0, 1, 2, etc.	index of coefficients in series solution

## Superscripts

o	initial value
---	---------------

## REFERENCES

1. L. P. White, *This Journal*, **130**, 1543 (1983).
2. L. P. White and N. Miskowski, *J. Vac. Sci. Technol.*, **B3**, 862 (1985).
3. L. P. White, *This Journal*, **132**, 168 (1985).
4. L. P. White, "Adv. Resist Technol. and Process, II," *SPIE*, **539**, 29 (1985).
5. L. P. White, *This Journal*, **132**, 3037 (1985).
6. R. H. Wilson and P. A. Piacente, *Semiconductor International*, **9**:4, 116 (1986).
7. R. H. Wilson and P. A. Piacente, *This Journal*, **133**, 981 (1986).
8. L. E. Stillwagon, R. G. Larson, and G. N. Taylor, *ibid.*, **134**, 2030 (1987).
9. P. C. Sukanek, *J. Imaging Technol.*, **11**, 184 (1985).
10. W. S. Overdiep, in "Physicochemical Hydrodynamics," B. D. Spalding, Editor (1980).
11. W. S. Overdiep, *Prog. Org. Coat.*, **14**, 159 (1986).
12. D. E. Bornside, C. W. Macosko, and L. E. Scriven, *J. Imaging Technol.*, **13**, 122 (1987).
13. S. Middleman, "Fundamentals of Polymer Processing," pp. 171-172, McGraw-Hill Book Co., New York (1977).
14. J. M. Shaw, M. A. Frisch, and F. Dill, *IBM J. Res. Dev.*, **28**, 210 (1977).
15. Anon, *Semiconductor International*, **10**:3, 24 (1987).

## Strain Adjustment in Si/SiGe Superlattices by a SiGe Alloy Buffer Layer

H.-J. Herzog, H. Jorke, and E. Kasper

AEG Research Center Ulm, D-7900 Ulm, Germany

S. Mantl

Institut für Festkörperforschung der KFA Jülich GmbH, D-5170 Jülich, Germany

### ABSTRACT

Strain distribution in a Si/Si<sub>1-x</sub>Ge<sub>x</sub> strained layer superlattice on Si can be adjusted by epitaxial insertion of a strain relieved homogeneous Si<sub>1-y</sub>Ge<sub>y</sub> buffer layer between the substrate and the superlattice. We report on the strain relief in Si<sub>1-y</sub>Ge<sub>y</sub> alloy buffer layers with  $y = 0.225$  as a function of layer thickness. The layers are grown by molecular beam epitaxy on (100) Si substrates at 450°C. X-ray diffraction, transmission electron microscopy, and Rutherford backscattering are applied to the film analysis. Above a critical thickness, i.e., the onset of strain relief, in a first range a strong decrease of film strain by formation of misfit dislocations is observed followed by a saturation-like branch with only a weak strain thickness dependency. A residual strain of about 1/3 of the lattice mismatch is found at a thickness of five times the critical one.

Presently, strained layer heterostructures and, particularly, strained layer superlattices (SLSs) are being studied for fundamental reasons as well as for device applications. Quantum size effects in such artificial, thin layer structures combined with the capability of tailoring the electronic and optical properties of the individual layers by controlling the magnitude of the strain enables a wide variety of high performance devices. Recently, the heterosystem Si-Ge with its relatively large lattice mismatch of about 4% has attracted particular attention. Since the early report on MBE grown Si/Si<sub>1-x</sub>Ge<sub>x</sub> SLSs on Si substrates by Kasper *et al.* (1) progress in Si MBE technique and development of appropriate doping methods have taken place [see for review Ref. (2)].

As an interesting result of these developments, Jorke *et al.* (3) reported the preparation of n-type modulation doped Si/Si<sub>0.5</sub>Ge<sub>0.5</sub> SLS grown atop an incommensurate Si<sub>0.75</sub>Ge<sub>0.25</sub> alloy buffer layer on an Si substrate. By using the buffer layer both the Si and the Si<sub>0.5</sub>Ge<sub>0.5</sub> superlattice constituents are under strain of opposite sign. This SLS showed enhanced room temperature electron mobility by formation of a two-dimensional electron gas in the Si layers. On the other hand, People *et al.* (4) published a p-type modulation doped Si/Si<sub>0.8</sub>Ge<sub>0.2</sub> SLS directly grown on an Si substrate with a two-dimensional hole gas in the SiGe alloy constituents. In this structure only the Si<sub>0.8</sub>Ge<sub>0.2</sub> layers are strained. The significance of using the buffer layer for the band alignment between the Si/Si<sub>1-x</sub>Ge<sub>x</sub> SLS inter-